Department of the Interior

U. S. Geological Survey

Coda duration magnitudes in central California: An empirical approach

by

Caryl A. Michaelson [1]

Open File Report 87-588

[1] Menlo Park, California

1987

CODA DURATION MAGNITUDES IN CENTRAL CALIFORNIA:

AN EMPIRICAL APPROACH

by

Caryl A. Michaelson

ABSTRACT.

A new empirical lapse time coda duration magnitude $\hat{M}_D$ is presented to establish the continuity of duration magnitudes in the central California seismic network during the period beginning from mid-1977 through 1981. $\hat{M}_D$ is modeled by relating Wood-Anderson or synthetic local magnitudes $\hat{M}_L$ to a polynomial function of $\log \tau$ (where τ is the lapse time duration measured from the earthquake origin time), a correction for the instrument attenuation setting of the seismograph station α, and a site correction $\overline{\delta}$ assumed to be related to the attenuation and scattering properties of the local geology. Previously coda durations were measured from the P-wave arrival time. The new formula for coda magnitude is based on data from 55 earthquakes in 5 source regions with $0.9 \leq \hat{M}_L \leq 5.6$, is $\hat{M}_D = -0.43\ (\pm 0.068) + 0.84\ (\pm 0.074) \log \tau + 0.56\ (\pm 0.020) \log^2 \tau + \alpha + \overline{\delta}$, and provides site corrections for 214 stations. The site corrections are spatially correlated. Stations overestimating $\hat{M}_D$ correspond to sites of lower density, and those underestimating $\hat{M}_D$ correspond to higher density sites, as indicated by the isostatic gravity field.

INTRODUCTION.

The primary purpose of this paper is to define an empirical coda magnitude estimate for the central California short-period seismic network (CALNET), by examining the relationship between coda durations and Wood-Anderson magnitudes, $\hat{M}_L$. A uniform estimate of earthquake magnitudes is essential for comparisons between different source regions and during different time periods. This is important for detecting and evaluating whether or not there are significant spatial or temporal variations in seismicity rates and attenuation. The continuity of magnitudes, particularly for such a large region, is made difficult by the sporadic nature of network operations and seismic activity.

Bakun [1984b] conducted a pilot study to establish a preliminary empirical relationship of coda magnitude with $\hat{M}_L$. Bakun [1984a] calculated Wood-Anderson magnitudes for the central California seismic network (CALNET) from Wood-Anderson or synthetic Wood-Anderson seismograms. He selected 110 earthquakes in 5 source regions with $0.7 \le \hat{M}_L \le 5.6$, during the period from mid-1977 through 1981. Based on 55 of these earthquakes, Bakun [1984b] used observations of traditional coda duration τ, epicentral distance Δ, and station corrections $\overline{\delta}$, from 42 CALNET stations recorded on develocorder film to obtain the following empirical formula:

$$\hat{M}_D = 0.92 + 0.607(\pm 0.005) \log^2 \tau + 0.00268(\pm 0.00012)\, \Delta + \overline{\delta},$$

with the event magnitude being the mean of the individual estimates. The station corrections, $\overline{\delta}$, are listed in Table 2 of Bakun [1984b].

The coda duration magnitude formulation presented in this study differs from Bakun's and other duration magnitudes in several ways. Most importantly, the duration is redefined as the lapse time duration, following a suggestion from Aki [personal communication, 1986], rather than the traditional coda duration. The lapse time duration τ, is the signal duration beginning with the event origin time, rather than the P-wave arrival time, as used in the traditional coda duration τ [Lee et al., 1972]. Thus, the two durations are related in the following way, $\tau = t_P + \tau$, where t_P is the P-wave travel-time. Using the lapse time duration has two distinct advantages: it relieves some of the problems associated with velocity model assumptions, and it inherently incorporates the distance term but is simpler to calculate than the (epicentral or hypocentral) distance. Other differences in the magnitude determination include the functional form of the magnitude relationship, and I applied corrections for

the average site characteristics and for the instrument attenuation setting of the seismograph station. Finally, the magnitude of an earthquake is represented by the weighted median of the individual estimates rather than their mean. The new coda magnitude is based on a function of the lapse time duration, instrument attenuation and site corrections, $\hat{M}_D \sim f(\log \tau, \alpha, \overline{\delta})$.

DATA.

The data included in this analysis are local Wood-Anderson or synthetic local magnitudes $\hat{M}_L$, duration measurements and phase data from CALNET stations recorded on develocorder film for 110 earthquakes in central California. The hypocenters and $\hat{M}_L$ magnitudes for these earthquakes were obtained from Tables 1-5 in Bakun [1984a]. Figure 1 is a map of the epicenters and the CALNET station locations used in this study. The insert in Figure 1 shows the depth distribution in each of the 5 source regions. For this paper I selected half of the earthquakes listed in Table 2, and systematically read from the develocorder film the P-wave arrival times and coda cutoff times at every CALNET station that recorded the events. In order to be consistent with the CALNET phase data base, I used the same coda cutoff criteria prescribed by Lee et al. [1972], whereby the end of the coda is the time when the coda envelope decreases to 10 mm peak-to-peak amplitude at a specific viewer magnification of 10 mm = 1 sec. (There are alternatives to this criteria, but the goal is to provide a magnitude formulation consistent with the CALNET coda readings during this time period.)

More than 5300 durations were measured initially; this is as complete a compilation as possible for these stations and set of events. Some of these data have been rejected based on a few simple rules. Durations read from traces where the P-wave travel-time residual is larger than ±2.0 seconds are deleted because there is a high probability that the seismic signal is not from the station associated with that channel (e.g. from cross-talk on the discriminators or misidentified channels). Durations whose measured lapse times are less than the expected S-wave travel-time t_S are also deleted because the coda is considered to be dominated primarily by scattered S-waves [Aki and Chouet, 1975]. The routine CALNET practice has been to reject coda durations with $\tau < 10$ sec because of the high probability that the signal is dominated by direct arrivals rather than scattered waves. By adopting the minimum travel-time criteria $\tau \geq t_S$, even codas of very short duration may be used. For typical

California crustal velocities, the S-wave travel-time is $t_S \approx 1.7\ t_P$. Figure 2 is a plot of log τ versus the P-wave travel-time with a curve corresponding to the minimum lapse time criteria $\tau = t_S$. A total of 5130 observations from 210 stations comprise the resulting data set henceforth referred to as the *independent set*.

The independent set is used to establish an empirical relationship between lapse time duration τ and local magnitude $\hat{M}_L$ through a weighted least-squares regression analysis. I restrict the observations in the regression analysis to a subset of the independent set that reflects the data distribution in the CALNET catalog. Specifically, the coda durations τ available from the CALNET data base are largely from stations that are within a radius of 100 km from the epicenter. Therefore, in this study the regression is restricted to observations from stations located within a P-wave travel-time radius of t_P = 17.5 sec ($\approx$ 100 km), and have errors that are less than the median absolute deviation, described later in this report. The resulting data set used in the regression include durations from 156 CALNET stations within a radius of t_P = 17.5 sec, with ten of them having less than 5 readings for the 55 shocks considered. The M_L for an additional 50 earthquakes obtained from Bakun [1984a,b] along with phase data and coda durations obtained directly from the CALNET catalog data base are referred to as the *test set*. The test set is used to help evaluate the new relationship determined from regression analysis, and is described later in this report.

ATTENUATION CORRECTION.

The coda duration formulations of Lee et al. [1972] and Bakun [1984a, 1984b] do not explicitly accommodate variations in seismograph magnification. In fact, for every change of 6 dB the signal amplitude changes by a factor of 2. Lee et al. [1972] considered the seismograph attenuation insignificant to the resultant magnitude, probably because most of their data were from a small range of attenuation settings. However, Bakun [1984b] noted a systematic correlation between the attenuation and the station corrections. In this study, the independent set has observations over a wide range of instrument attenuation settings from 6 dB to 42 dB. Hence the signal amplitude may vary by as much as a factor of 2^6, affecting the cutoff time of the duration significantly. Thus, the apparent magnitude may vary by a factor of log 2^6 = 1.8, due to different instrument attenuation settings alone. In most cases, the instrument attenuation is set according to the observed seismic background noise at

each site, so that recorded background levels are relatively uniform across the network. The seismic background noise is usually related to the local geology except at locations near the sea coast, or where cultural or atmospheric noise levels are high.

I isolated the instrument attenuation as a separate correction term α, in the magnitude formula so that the site corrections $\overline{\delta}$ reflect local geological site characteristics as much as possible. According to Richter [1935], the amplitude of an earthquake signal decays at a constant rate, $A_t \sim A_o\, t^{-q}$, where A_t is the amplitude at time t from signal origin, A_o is related to the source function, and q is a constant. Johnson [1979] suggested that the amplitude decay rate is dependent on the site geology and the attenuation factor Q, calculating $0.8 < q < 2.2$ for most southern California stations. Unfortunately, Johnson did not distinguish the seismograph instrument attenuation from site characteristics. The magnitudes of Johnson's earthquakes were limited to $2.0 \le M_L \le 4.5$, so that q may be more complicated over a wider magnitude range. Lindh [personal communication, 1987] has found a range of q=2-3 for the Parkfield, California region.

Varying the instrument attenuation affects the time required for the signal amplitude to decay by a factor of 2 for each 6 dB setting. The difference in time is related to $\Delta \log t \sim \frac{\Delta \log A}{q} = \frac{\log 2.0}{2.0} = 0.15$ per 6 dB, assuming q=2.0. Geometrically, this is illustrated in Figure 3, where plots of log A versus log t are straight lines with slope $-q = \frac{\log A}{\log t}$. While the difference in the amplitude magnitude estimate would change by a factor of $\Delta M_L \sim \Delta \log A$, the duration magnitude changes by a factor of $\Delta M_D \sim \Delta \log t = \frac{\Delta \log A}{q}$, Consequently, variations in signal duration and apparent duration magnitude due to a change in the instrument attenuation setting is $\Delta M_D \sim \Delta \log t = 0.0250$ per dB. Eaton [1984] noted that the majority of CALNET stations have attenuation settings of 12 dB and 18 dB, and suggested that the average for the network be considered 15 dB, although this is not an actual instrument setting. Assuming the attenuation correction is zero at 15 dB, I adopt the following linear relationship:

$$\alpha_{ij} = \frac{\log 2.0}{2.0}\,\frac{attn_{ij}}{6\text{dB}} + c = 0.025\, attn_{ij} - 0.375, \qquad (4)$$

for the j^{th} station at the time of the i^{th} earthquake, with q=2.0. (For q=3.0, $\alpha_{ij} = 0.017\, attn_{ij} - 0.255$.) Because I use a quadratic form of τ in the estimate of M_D, α may be better estimated by a quadratic, but the difference

between the two is small. The attenuation settings may be obtained from the CALNET station maintenance history files that are described by Eaton [1986]. The stations used in this study are of the same instrument type. If any other type were to be included, differences in the instrument response may require a further magnitude adjustment.

REGRESSION ANALYSIS.

Model. The coda magnitude relationship presented in this paper is derived from the results of a standard procedure of stepwise, linear, weighted least-squares regression and exploratory data analysis [Mosteller and Tukey, 1977]. The fundamental goal is to relate lapse time coda durations $\tilde{\tau}$ to Wood-Anderson magnitudes. Obtaining the "best" fit involves a number of competing criteria, and the first problem is choosing an appropriate model. I tested several classes of models that included parameters other than the lapse duration, attenuation and $\overline{\delta}$, specifically distance, focal depth, and azimuth. I monitored the data variance and other statistical measures while systematically introducing the predictor variables of varying order. In the end, I concluded that M_D is adequately modeled by a quadratic polynomial of log $\tilde{\tau}$, with the site and instrument attenuation corrections as additive constants. If the traditional coda duration, τ, had been used instead of the lapse duration, $\tilde{\tau}$, then it would be essential to include P-wave travel-time or some measure of distance (e.g. ray-path, hypocentral or epicentral distance and depth) as explicit predictor variables.

$\hat{M}_D$ requires a polynomial function of log $\tilde{\tau}$ because a linear function is not adequate over the large range of $\hat{M}_L$ values. As previously described, the independent set has magnitudes in the range from $0.9 \le \hat{M}_L \le 5.6$. If $\hat{M}_D$ is constrained to be linear in log $\tilde{\tau}$, it can adequately fit $\hat{M}_L$ over a limited range, approximately $2.0 < \hat{M}_L < 3.5$. On the other hand, if $\hat{M}_D$ is constrained to be linear in $\log^2 \tilde{\tau}$, it fits $\hat{M}_L$ over a larger range, approximately $1.5 < \hat{M}_L < 4.0$. However, by including both $\log^2 \tilde{\tau}$ and log $\tilde{\tau}$ terms, $\hat{M}_D$ fits $\hat{M}_L$ quite well over the full range of magnitudes in the independent set. Table 1 summarizes the analysis of variance after regression of several classes of models in which increasing orders of log $\tilde{\tau}$ are introduced. While all of the models yield similar magnitudes and fit about 89-97% of the data variance, the simplest model to "adequately" accomplish the job is desired. A few points should be noted that helped direct the final choice of model. Models of class B,

$M_D \sim f(\log^2 \tau)$, have smaller standard errors and fits the data better than models of class A, $M_D \sim f(\log \tau)$. However, models of class C, $M_D \sim f(\log \tau, \log^2 \tau)$, fit the data better than either models of class A or B. Higher orders of $M_D \sim f(\log^n \tau)$, with $n \geq 3$, do not increase the overall fit of the data, or reduce either the data variance or the standard errors significantly. This can be seen in the class D model, which does not improve the fit significantly over the equivalent class C model. Within each class, both the attenuation and site corrections enhance the solutions approximately 1% and 4% respectively. Using these criteria, I adopted the following formula:

$$\hat{M}_{D_{ij}} = a_0 + a_1 \log \tau_{ij} + a_2 \log^2 \tau_{ij} + \alpha_{ij} + \overline{\delta}_j, \tag{5}$$

where τ_{ij} is the total lapse time in seconds observed at the j^{th} station for the i^{th} earthquake, α_{ij} is the instrument attenuation correction and $\overline{\delta}_j$ is the site correction.

Weighting. The independent set does not have uniform distribution in terms of source magnitude, depth, source-station distance, azimuth, and site geology. Nor does it have the same data distribution as the CALNET catalog. The majority of earthquakes in the CALNET catalog have magnitudes less than 2, therefore it is important to estimate them as well as possible without sacrificing the fit to large magnitude events. By comparison, the independent set is relatively depleted in small magnitude earthquakes, and has observations from stations at distances up to 4-5 times greater than are normally included in the catalog.

Considering these differences, weights are assigned to each observation in the following manner. The weighting vector is inversely proportional to the sum of the individually assigned weights, $\mathbf{W} \sim \sum w^{-1}(M_L, t_P)$. Note that this is different from the standard statistical approach where weights are inversely proportional to the variance, which is known from the whole population distribution, and the sample population has the same distribution. I assigned individual weights according to the number of observations in small ranges of magnitude N_{M_L} and travel-time N_{t_P}. The magnitude weight is $w_{M_L} = \sum_{\beta_i}^{\beta_{i+1}} N_{M_L}$ for the magnitude range $\Delta M_L = \beta_{i+1} - \beta_i = 0.2$. This mitigates the problem that earthquakes of small magnitudes have fewer observations than larger events, and balances the total number of earthquakes in each magnitude range. The weight assigned to the travel-time observations is done in a similar manner: $w_{t_P} = \sum_{\gamma_i}^{\gamma_{i+1}} N_{t_P}$ in the travel-time range $\Delta t_P = \gamma_{i+1} - \gamma_i = 2.5$ sec for

$t_P \leq 17.5$ sec, and $w_{t_P} = \infty$ for $t_P > 17.5$ sec. In practice, observational data at distant stations $t_P > 17.5$ sec and with large standard errors are excluded from the regression analysis for reasons mentioned earlier. The weights may be augmented according to other observations if their distribution significantly biases the problem. Thus, the weights chosen provide uniform weighting over the magnitude range $0.9 \leq M_L \leq 5.6$ and the P-wave travel-time range $0.0 \leq t_P \leq 17.5$ sec.

Results. The final formula is the result of an iterative process whereby site corrections are calculated from the average station misfit from an initial magnitude formula, and are then included as a constant in the regression to obtain a better fitting solution. After 3 iterations, the ratio of the fit variance to the data variance R^2, converged to a stable maximum, and the variance and standard errors converged to stable minima. The constant coefficients are: a_0=–0.4259 (±0.0681), a_1=0.8442 (±0.0743), a_2=0.5572 (±0.0199), and $\alpha_{ij} = (0.025\ attn_{ij} - 0.375)$, so that Equation (5) becomes:

$$\hat{M}_{D_{ij}} = -0.43\ (\pm 0.068) + 0.84\ (\pm 0.074) \log \tau_{ij} + 0.56\ (\pm 0.020) \log^2 \tau_{ij} + \alpha_{ij} + \overline{\delta}_j, \qquad (6)$$

This relationship accounts for 97.0% of the data variance, compared to 93.4% claimed by Lee et al. [1977] and 91.5% by Bakun [1984b].

Appendix A contains histograms of $\hat{M}_{D_{ij}}$ for all of the data for each earthquake to compare the mean, median and mode as estimates of central tendency. The weighted median $<M_D>$, and the median absolute deviation MAD, are chosen as the measures of central tendency and spread, rather than the mean and standard error. MAD is the median value of the absolute deviations between the individual estimates and the event median, $MAD = \text{median} \left| \hat{M}_{D_{ij}} - <M_D>_i \right|$ [Mosteller and Tukey, 1977]. Alternatively, a more robust estimate of the MAD may be selected. The median is chosen because it is not as sensitive as the mean to individual outliers. By inspection of the $\hat{M}_D$ histograms, there is not much difference between the measures of central tendency. However, for earthquakes with few or a skewed distribution of observations, the median is closer to an intuitive estimate of the desired central tendency than the mean. The MAD also gives a better estimate of spread or uncertainty under these circumstances than the standard deviation or confidence limits. Also, the median and MAD are easily determined. Figure 4 is a plot of $<M_D> \pm MAD$ including all of the observations, versus $\overline{M}_L \pm 95\%$ confidence limits from Bakun [1984a]. All of the $\hat{M}_D$ estimates are within the error MAD of the $\overline{M}_L$ estimates.

Table 2 lists the magnitude estimates where Equation (6) is applied to all of the observations with (a) $t_P \leq 17.5$ sec, and (b) all t_P. The modal value is also an acceptable measure of central tendency, but the maximum of a continuous function representing the distribution, or the maximum likelihood, must be found first, and while this is simple, it is cumbersome to calculate for large numbers of earthquakes. The three measures of central tendency yield consistent estimates when there are numerous observations per event. The estimates are also consistent when including stations from the entire range of t_P even though Equation (6) was based on stations in a limited range of t_P. Only in 2 cases do the magnitude estimates based on $t_P \leq 17.5$ sec and all t_P differ by more than 0.05, and for these 2 instances, the difference is 0.08 $\hat{M}_D$. For virtually all but one, the difference is less than the error estimated by the *MAD*. Thus, it is reasonable to suggest that including all t_P in the median does not bias the estimate of $\hat{M}_D$.

MAGNITUDE MISFIT.

The distribution of error in estimating $\hat{M}_D$ is another indication of how well the relationship fits the data. The magnitude misfit, ε_{ij}, is defined as the difference between the magnitude calculated from a single station and the true magnitude. I estimate the misfit as the deviation from the median, $\hat{\varepsilon}_{ij} = \hat{M}_{D_{ij}} - \langle M_D \rangle_i$. In Figure 5, the misfit is plotted against the following parameters: log τ, observed P-wave travel-time, epicentral distance, and azimuth. The data included in these plots are not restricted in range of t_P. As can be seen in Figure 5, about 90-95% of the data are within 1/4 of a magnitude unit of the median represented by $\hat{\varepsilon} = 0.0$. In Figure 5(a), $\hat{\varepsilon}$ is plotted versus log τ. Most of the data lie in the range log τ = 1.25-2.60. The scatter is fairly uniform, although slightly less at log τ = 1.75-2.25. In general, the misfit is uncorrelated over the range of $10 < \tau < 550$ seconds. In Figure 5(b), $\hat{\varepsilon}$ is plotted versus P-wave travel-time, t_P. While only data with $t_P \leq 17.5$ sec were used for the regression, the data from stations beyond this radius are fit equally well. The scatter actually decreases for $t_P > 25.0$ sec, although this may be attributed in part to the fewer data beyond this radius. Likewise, the scatter of $\hat{\varepsilon}$ decreases with increasing epicentral distance beyond about 150 km, as shown in Figure 5(c). Thus, I conclude that Equation (6) may be extrapolated to τ over the full range of t_P without systematically biasing the magnitude. In Figure 5(d), $\hat{\varepsilon}$ is plotted versus the azimuth from the epicenter to the station location. The clustering of data in the NW and SE directions reflects the distribution of stations in northern California and events in

the independent set. In addition, by inspection of Figure 4, neither the *MAD* nor the deviation of the median from $\overline{M}_L$ are related to increasing $\hat{M}_L$. The difference between $<M_D>$ and $\overline{M}_L$ are plotted versus depth in Figure 6. While there are not enough earthquakes in the independent set to infer anything about a depth dependence, there is a hint of a pattern. The difference tends to be slightly negative at depths of 7-10.5 km and at 12-15 km, indicating that $\hat{M}_D$ slightly underestimates $\hat{M}_L$ in these depth ranges. At depths shallower than 7 km, the coda magnitudes are slightly greater than $\hat{M}_L$. In summary, the data misfit is small and uncorrelated as a function of log τ, observed P-wave travel-time, epicentral distance, source-receiver azimuth and $\hat{M}_L$. The misfit is uniformly distributed, and does not appear to be attributable to systematic biases in the data, the choice of weighting in the regression analysis, or by the formula for $\hat{M}_D$ given in Equation (6). There appears to be a weak correlation with depth, but this may be related to the material properties in the upper crust as a function of depth.

SITE CORRECTIONS.

The site correction, $\overline{\delta}$, is the mean of the difference between the event magnitude and individual station estimates:

$$\overline{\delta}_j = \frac{1}{K}\sum_{i=1}^{K}[\ <M_D>_i - \hat{M}_{D_{ij}}\ ],$$

where K is the number of events station j has observed. Site corrections for stations outside the P-wave travel-time radius of 17.5 seconds were assigned the negative of the mean magnitude misfit, $-\overline{\varepsilon_{ij}} \rightarrow \overline{\delta}_j$. These site corrections are preliminary and are denoted by asterisks in Table 3. Similarly, additional site corrections may be assigned on a tentative basis to this list as stations are added in future applications. There are observations at 156 stations within the $t_P \leq 17.5$ sec. Ten of the 156 stations are represented by fewer than 5 earthquakes. In the entire independent set, there are observations at 214 stations, with 34 of them recording fewer than 5 earthquakes.

As the seismograph characteristics are not incorporated in the site corrections, it may be possible to infer geological and geophysical relationships from the spatial and temporal patterns apparent in the site corrections. The magnitude misfit $\hat{\varepsilon}_{ij}$ and the site corrections $\overline{\delta}_j$ are plotted versus the average of the attenuation settings per station in Figure 7. Negative and positive corrections represent sites that typically over- and underestimate

earthquake magnitudes respectively. Site corrections are shown in map view in Figure 8. Open symbols represent sites that typically overestimate the average magnitude of earthquakes and have negative $\overline{\delta}$. Solid symbols represent sites with positive $\overline{\delta}$ that typically underestimate the magnitude of earthquakes.

The site correction is spatially correlated with local geology. Sites that are located on hard rock sites (e.g. granites, ultramafics, metamorphosed Mesozoic sediments) and fast P-wave crustal velocities, tend to underestimate $\hat{M}_D$ and have positive $\overline{\delta}$. Sites located on Cenozoic volcanics and unmetamorphosed Mesozoic sediments do not have clear affinities. I adopted the geologic code of Evernden, Kohler and Clow [1981], in an attempt to quantify the correlation between the site correction and local geology. Evernden, Kohler and Clow [1981] divide the surficial geology in California into 10 geologic units. Granitic and metamorphic rocks are represented as (A). Paleozoic to Quaternary age sedimentary rocks are represented by (B) through (F) and (J). Tertiary and Quaternary volcanic rocks are (H) and (I) respectively. I denote rocks of unknown type by the letter (U). The site corrections are plotted against the code for the mapped surficial geology in Figure 9 (top). Granitic and metamorphic rocks typically have positive corrections, $\overline{\delta} \approx 0.15 \pm 0.30$. Early Mesozoic sediments have $\overline{\delta} \approx 0.00 \pm 0.35$. Early Tertiary sediments have $\overline{\delta} \approx 0.20 \pm 0.20$. Oligocene-Pliocene sediments have $\overline{\delta} \approx 0.05 \pm 0.50$. Quaternary sediments have a large range of values, roughly $\overline{\delta} \approx 0.00 \pm 0.75$. Tertiary and Quaternary volcanic rocks tend to have negative values, $\overline{\delta} \approx -0.20 \pm 0.45$ and $\overline{\delta} \approx -0.30 \pm 0.40$. The older Paleozoic and early Mesozoic sediments (B) and (C), tend to overestimate $\hat{M}_D$ compared to the younger early Tertiary through Pliocene sediments (E) and (F), while the youngest Quaternary sediments (J), have the greatest range of values. Conversely, the older Tertiary volcanics (H) tend to underestimate $\hat{M}_D$ compared to the younger Quaternary volcanics (I), although their range of values overlap quite a bit. A correlation of $\overline{\delta}$ with age of the rocks might be inferred, but the relation is weak, and is opposite in sediments and volcanic rocks.

The site correction is spatially correlated with rock density in the upper crust. In Figure 9 (bottom), the site correction is plotted versus the isostatic gravity field interpolated for that location, obtained from Jachens and Griscom [1985]. Stations over sites with relatively low gravity anomalies tend to overestimate earthquake magnitudes, while sites with relatively high gravity anomalies tend to underestimate $\hat{M}_D$. This suggests that rocks of low density material tend to ring longer than the high density rocks when excited by seismic frequen-

cies.

TEST SET.

The coda magnitude relationship may be further evaluated by applying the formula to a different set of data in which the local magnitudes are known *a priori*. I used 50 of Bakun's [1984a,b] earthquakes not already included in the independent set for which $\hat{M}_L$ has already been established, and applied Equation (6) and the site corrections from Table 3 to the duration measurements available from the CALNET catalog. Hereafter these events are referred to as the *test set*. To obtain the lapse time duration τ, I simply added the observed P-wave travel-time t_P, to the catalog of CALNET coda durations τ, such that the new lapse durations are the linear combination $\tau = \tau + t_P$. The magnitudes for the test set are listed in Table 4, and in Figure 10, $<M_D>$ is plotted against $\overline{M}_L$. The magnitude relationship represented by Equation (6) accounts for about 90-95% of the data variance in the test set, with the *MAD* generally less than 0.15 $\hat{M}_D$.

The test set may also be used to evaluate how the distribution of the duration readings in the CALNET data base influences the magnitude estimates during the period from mid-1977 to 1981. It is important to note that the lapse time coda durations for the test set of earthquakes were obtained directly from the readings of the CALNET data base, relying on the routine processing of these earthquakes done by the U.S.G.S. staff. No attempt was made to expand the number of data available or to evaluate individual readings. The test set consists of few τ per event because the CALNET catalog is relatively sparse in duration measurements. There are a total of 1016 observations of τ at 144 stations included in the test events. These include all observations of t_P because of the few total number of data available. There are few data (33) in the radius between $t_P > 17.5$ sec and $t_P < 25.0$ sec, and none beyond. Thus, the magnitudes are not biased due to the inclusion of these data.

The magnitude misfit for the test set is plotted in Figure 11 versus (a) log τ, (b) t_P and (c) azimuth. I omit the plot of the misfit versus epicentral distance because it is redundant of the plot versus P-wave travel-time. As can be seen in Figure 11, about 90-95% of the data are within 1/4 of a magnitude unit of the median represented by $\hat{\varepsilon} = 0.0$. As with the misfit for the independent data, the data misfit is small and uncorrelated as a function of log τ, observed P-wave travel-time, or source-receiver azimuth. The magnitudes for the test set tend to overesti-

mate the Wood-Anderson magnitudes by approximately 0.10-0.15 $\hat{M}_D$ units (see Figure 10). This is partly due to the higher proportion of events at depths shallower than 7 km in the test set than are in the independent set. Also, because the CALNET database tended to exclude coda durations less than 10 sec, the event magnitude would be biased to a larger estimate, perceptible only at small magnitudes. As with the independent set, there appears to be a weak correlation of the difference $<M_D> - \overline{M}_L$ with depth (Figure 11 (d), but this is probably related to the properties in the upper crust. As observed with the independent set, earthquakes at 7-10 km depth have $\hat{M}_D$ magnitudes that tend to underestimate $\hat{M}_L$, and there are fewer of these proportionately in the test set. In summary, the misfit of the test set is small and uniformly distributed. Equation (6) estimates the magnitude of the test set of earthquakes almost equally as well as for the independent set despite the difference in the number of data available for the test set. There do not appear to be any systematic biases in the CALNET data base that are unaccounted for in the weighting assigned in the regression analysis. The only exception to this is the weak correlation with depth. Because this cannot be modeled as a smooth function, a large number of earthquakes should be examined carefully before attempting to interpret it any further.

SUMMARY.

A new empirical coda duration magnitude relationship is presented to help establish the continuity of earthquake magnitudes throughout the central California seismic network during the period from mid-1977 through 1981. $\hat{M}_D$ is based on a quadratic polynomial function of log τ (where τ is the lapse time duration), a correction for the attenuation setting of the seismograph instrument, and a site correction assumed to be related to the characteristic attenuation properties of the local geology. $\hat{M}_D$ has been modeled against Wood-Anderson and synthetic local magnitudes, so that any discontinuities or systematic biases in the M_L scale will be incorporated into $\hat{M}_D$. The new formula for $\hat{M}_D$ appears to work well when applied to the CALNET data base, despite the relatively few number of coda duration measurements in the catalog per earthquake. Considering the limited number of durations in the CALNET data base, a large number of events should be examined to determine whether there are more complex spatial (or temporal) patterns than briefly mentioned in this study. However, extrapolation of $\hat{M}_D$ to other stations and earthquakes outside these 5 source regions should be approached cautiously.

REFERENCES.

Aki, K., and B. Chouet, Origin of coda waves: source, attenuation and scattering effects, *J. Geophys. Res. 80*, 3322-3342, 1975.

Bakun, W. H., Seismic moments, local magnitudes and coda-duration magnitudes for earthquakes in central California, *Bull. Seismol. Soc. Am. 74*, no. 2, 439-458, 1984.

Bakun, W. H., Magnitudes and moments of duration, *Bull. Seismol. Soc. Am. 74*, no. 6, 2335-2356, 1984.

Draper, N. and H. Smith, Applied regression analysis, 2nd edition, *John Wiley and Sons*, 709pp., 1981.

Eaton, J. P., Content and structure of the CALNET location history file, LOCHST, and the CALNET maintenance history file, MNHST, *U.S.G.S. Administrative Report*, 15pp., 1986.

Eaton, J. P., Noise analysis of the seismic system employed in the northern and southern California seismic nets, *Open-file Report 84-657*, 23pp., 1984.

Evernden, J. F., W. M. Kolher, and G. D. Clow, Seismic intensities of earthquakes of conterminous United States - Their prediction and interpretation, *Geol. Surv. Prof. Paper 1223*, 56pp., 1981.

Jachens, R. C., and A. Griscom, An isostatic residual gravity anomaly map of California - A residual map for interpretation of anomalies from intracrustal sources, in Hinze, W. J., *ed.*, The utility of regional gravity and magnetic anomaly maps, Soc. of Explor. Geophys., Tulsa Oklahoma, 347-360, 1985.

Johnson, C. E., I. CEDAR - An approach to the computer automation of short-period local seismic networks, II. Seismotectonics of the Imperial Valley of southern California, Ph.D. Dissertation California Institute of Technology, 332pp., 1979.

Lee, W. H. K., R. E. Bennett and K. L. Meagher, A method of estimating magnitude of local earthquakes from signal duration, *Open-file Report*, 28pp., 1972.

Mosteller, F. and J. W. Tukey, Data analysis and regression, *Addison-Wesley*, 588pp., 1977.

Richter, C. F., An instrumental earthquake magnitude scale, *Bull. Seismol. Soc. Am. 25*, 1-32, 1935.

ACKNOWLEDGEMENTS.

I would like to express my appreciation to Bill Bakun for his support and critical comments throughout this project. Choosing the best fitting model requires intimate knowledge of the network operations in CALNET, detection thresholds, and a thorough familiarity with the seismicity distribution in space and time. Because of the massive volume of data and the complexity of the problem, I relied on the considerable knowledge of Kei Aki, Bill Bakun, Jerry Eaton, Bill Ellsworth, Fred Klein, Rick Lester, Al Lindh, Shirley Marks, and Dave Oppenheimer. Bob Simpson provided the gravity data and geologic codes used in the figures.

TABLES.

Table 1. Analysis of variance. The standard error of the residuals, SE; the data variance, $\sum(res)^2$; the ratio of the fit variance to the data variance, R^2; improvement over a model with no variables, F-test; and the number of degrees of freedom, NDF [Draper and Smith, 1981; Mosteller and Tukey, 1977] are reported for each model.

Table 2. Magnitude estimates for earthquakes in the independent set. Refer to Tables 1-5 in Bakun [1984] for the source parameters. Regions (1) Parkfield, (2) San Juan Bautista, (3) Sargeant Fault, (4) Coyote Lake, and (5) Livermore are the same as in Figure 4.

Table 3. Site corrections. An asterisk indicates that the estimate for this station comes from earthquakes at distances greater than the P-wave travel-time of $t_P \geq 17.5$ sec. Stations denoted with asterisks or those with fewer than 5 observations are suspect, and should be used with caution. A standard error listed as a question mark indicates that the quantity is undefined because this station is represented by only 1 observation.

Table 4. Magnitude estimates for earthquakes in the test set. Refer to Tables 1-5 in Bakun [1984] for the source parameters. Regions are the same as in Table 2.

FIGURE CAPTIONS.

Figure 1. Epicenters and CALNET stations used in this study. The earthquakes occured between mid-1977 through 1981. The independent set of earthquakes are denoted by squares, the test set are denoted by circles, and stations are noted as triangles. Wood-Anderson magnitudes are taken from Bakun [1984a]. The insert shows the depth distribution in each of the 5 source regions.

Figure 2. Log τ versus observed P-wave travel-time measured for the independent set of earthquakes. The solid curve represents the minimum $\tau = t_S$ criteria, where t_S is the expected S-wave travel-time. The symbol type indicates the source region (1) circle = Parkfield, (2) triangle = San Juan Bautista, (3) cross = Sargeant Fault, (4) X = Coyote Lake, and (5) diamond = Livermore, and are adopted in subsequent figures.

Figure 3. Signal amplitude as a function of time, in linear (top) and log space (bottom). Decreasing the instrument attenuation of the seismograph by 6 dB increases the signal amplitude by a factor of 2. The associated difference in duration of the signal is obtained through the relationship $\Delta \log t \sim -\frac{\Delta \log A}{q}$.

Figure 4. $<M_D>$ versus Wood-Anderson and synthetic local magnitude $\overline{M}_L$ for the 55 earthquakes in the *independent set.* Vertical and horizontal bars represent the median absolute deviation *MAD*, and the 95% confidence limits of $<M_D>$ and $\hat{M}_L$ respectively. $<M_D>$ for the 5 earthquakes with $\hat{M}_L \leq 1.5$ slightly overestimate $\hat{M}_L$, but the differences $<M_D> - \overline{M}_L$ are well within the error estimate, *MAD*.

Figure 5. Magnitude misfit $\hat{\varepsilon}_{ij} = \hat{M}_{D_{ij}} - <M_D>_i$ versus (a) log τ_{ij}, (b) P-wave travel-time $t_{P_{ij}}$, (c) distance Δ_{ij}, and (d) azimuth. Symbol types are the same as in Figure 4. Large (small) symbols represent data that are within (exceed) $\pm$ *MAD* of that individual event.

Figure 6. Magnitude misfit per event $<M_D>_i - \overline{M}_{L_i}$ versus source depth. Symbols are the same as Figure 4.

Figure 7. Top: Magnitude misfit $\hat{\varepsilon}_{ij}$ versus the instrument attenuation setting $attn_{ij}$ at the time of the i^{th} earthquake and at the j^{th} station. Bottom: Site correction $\overline{\delta}_j$ versus the average of the attenuation settings at the j^{th} station. (For example, if station XXX was set at 6 dB through 1980 and recorded 4 earthquakes in this time, but was then changed to 12 dB and recorded 2 earthquakes since 1981, then the average attenuation setting of station XXX for these 6 earthquakes is 8 dB.) Negative and positive corrections indicate sites that typically overestimate and underestimate earthquake magnitudes respectively.

Figure 8. Site corrections $\overline{\delta}_j$ in map view. Negative corrections (open symbols) represent sites that typically overestimate earthquake magnitudes. Positive corrections (filled symbols) represent sites that typically underestimate earthquake magnitudes. The symbol size is proportional to the absolute value of the station correction, the larger symbols have greater corrections. Stations with standard errors less than 0.25 or that recorded more than 5 events are denoted as squares, all others are denoted as circles.

Figure 9. Top: Site corrections $\overline{\delta}_j$ versus geologic code of Evernden, *et. al* [1981]. A = granitic and metamorphic rocks; B = Paleozoic sediments; C = Early Mesozoic sediments; D = Cretaceous-Eocene sediments; E = Early Tertiary sediments; F = Oligocene-Pliocene sediments; J = Quaternary sediments; H = Tertiary volcanics; I = Quaternary volcanics; U = rocks of unknown affinities. Bottom: Site corrections $\overline{\delta}_j$ versus the isostatic residual gravity field in milligalls taken from Jachens and Griscom [1985]. Symbols refer to the geologic code in the top diagram.

Figure 10. $<M_D>$ versus Wood-Anderson and synthetic local magnitude $\overline{M_L}$ for the *test set*. Symbols are the same as Figure 4.

Figure 11. Magnitude misfit $\hat{\varepsilon}_{ij} = \hat{M}_{D_{ij}} - <M_D>_i$ for the test set versus (a) log τ_{ij}, (b) P-wave travel-time $t_{P_{ij}}$, (c) azimuth and (d) depth. Symbols are the same as in Figure 4.

Appendix A. Frequency of magnitude estimates $\hat{M}_D$ for each earthquake in the independent set. $\hat{M}_L \pm 95\%$ confidence intervals obtained from Bakun [1984b] are plotted as inverted arrows and horizontal bars at the top

of each histogram. Beneath $\hat{M}_L$ are plotted the 3 measures of central tendency and error of M_D calculated in this study: the mode, the median $<M_D> \pm MAD$, and the mean $\overline{M_D} \pm 95\%$ confidence intervals. The number of duration measurements, N, are also listed. The event numbers (same as in Table 2) are printed in the upper right corner of each diagram. The width of the M_D window is 0.2 if N is less than 30, otherwise 0.1 is set as the width of the window. The + symbols represents a weighted 3-point running average of the frequency distribution of M_D estimates used to estimate the mode.

Appendix B. Frequency of magnitude estimates $\hat{M}_D$ for each earthquake in the test set. The event numbers correspond to those in Table 4. See Appendix A for explanation of the diagrams.

Table 1. Analysis of variance. The standard error of the residuals, SE; the data variance, $\sum(res)^2$; the ratio of the fit variance to the data variance, R^2; improvement over a model with no variables, F-test; and the number of degrees of freedom, NDF [Draper and Smith, 1981; Mosteller and Tukey, 1977] are reported for each model.

CLASS	MODEL	VARIABLES					ANALYSIS OF VARIANCE				
		LOG^n TAU , n = 1	2	3	G	$\bar{\delta}_j$	SE	R^2	$\sum RES^2$	F-TEST	NDF
A	1	✓					.01403	0.8935	0.6098	2.5989	3097
	2	✓			✓		.01322	0.9036	0.5415	2.9023	3097
	3	✓				✓	.01030	0.9426	0.3285	2.5441	3096
	4	✓			✓	✓	.008293	0.9621	0.2129	3.9285	3096
B	5		✓				.01341	0.9028	0.5567	2.8766	3097
	6		✓		✓		.01253	0.9134	0.4866	3.2651	3097
	7		✓			✓	.009728	0.9488	0.2930	2.8713	3096
	8		✓		✓	✓	.007560	0.9685	0.1769	4.7587	3096
C	9	✓	✓				.01338	0.9032	0.5546	1.4437	3096
	10	✓	✓		✓		.01252	0.9137	0.4849	1.6383	3096
	11	✓	✓			✓	.009608	0.9501	0.2857	1.9647	3095
→	12	✓	✓		✓	✓	.007408	0.9698	0.1699	3.3081	3095
D	13	✓	✓	✓	✓	✓	.007409	0.9698	0.1698	2.4807	3094

Table 2. Magnitude estimates for earthquakes in the independent set. Refer to Tables 1-5 in Bakun [1984] for the source parameters. Regions (1) Parkfield, (2) San Juan Bautista, (3) Sargeant Fault, (4) Coyote Lake, and (5) Livermore are the same as in Figure 4.

EV	DATE	REG	#OBS	MEDIAN+-MAD	MEAN+-95%	MODE	ML+-95%	#OBS	MEDIAN+-MAD
1	770621 0243	5	71	4.474 0.111	4.479 0.042	4.459	4.600 0.000	149	4.506 0.118
2	770622 1614	5	13	1.600 0.247	1.625 0.159	1.441	1.670 0.210	13	1.619 0.142
3	770623 1936	5	56	2.137 0.078	2.152 0.032	2.118	2.200 0.090	75	2.171 0.054
4	780921 0318	3	74	2.828 0.087	2.841 0.033	2.793	3.000 0.090	115	2.862 0.097
5	790111 1957	3	62	3.219 0.090	3.202 0.028	3.264	3.100 0.050	110	3.235 0.103
6	790218 0138	3	83	2.706 0.066	2.708 0.021	2.709	2.500 0.050	125	2.738 0.067
7	790807 0155	4	69	1.982 0.107	1.991 0.031	1.965	2.180 0.100	80	2.015 0.124
8	790807 0232	4	82	2.879 0.069	2.888 0.025	2.869	2.900 0.050	129	2.910 0.088
9	790807 0525	4	48	1.609 0.141	1.598 0.051	1.482	1.610 0.010	48	1.660 0.159
10	790807 0556	4	83	2.903 0.053	2.914 0.017	2.891	3.000 0.060	129	2.939 0.069
11	790807 0731	4	72	2.424 0.044	2.413 0.017	2.428	2.400 0.040	104	2.456 0.048
12	790809 1249	4	78	3.354 0.075	3.344 0.024	3.391	3.400 0.020	147	3.387 0.083
13	790810 0025	4	83	3.608 0.068	3.598 0.024	3.630	3.600 0.040	151	3.643 0.066
14	790819 0206	4	56	1.807 0.096	1.817 0.032	1.797	1.650 0.070	63	1.830 0.104
15	790819 0442	4	46	1.547 0.091	1.550 0.043	1.534	1.290 0.070	50	1.575 0.103
16	790914 0104	3	82	3.001 0.064	2.996 0.019	3.017	3.200 0.070	134	3.024 0.075
17	791004 1801	1	17	2.174 0.063	2.163 0.045	2.166	2.240 0.020	35	2.089 0.050
18	791004 1805	1	15	2.185 0.072	2.177 0.064	2.232	2.280 0.020	34	2.129 0.080
19	791114 0613	3	75	2.410 0.076	2.414 0.020	2.404	2.400 0.110	109	2.446 0.074
20	791203 2105	1	15	1.708 0.095	1.684 0.057	1.643	1.610 0.080	21	1.630 0.078
21	800125 0314	5	61	2.622 0.067	2.615 0.022	2.630	2.700 0.050	107	2.618 0.076
22	800125 0521	5	69	3.278 0.059	3.289 0.022	3.272	3.400 0.080	143	3.320 0.068
23	800125 0524	5	73	4.671 0.081	4.679 0.033	4.675	4.600 0.100	162	4.674 0.096
24	800125 0529	5	65	3.411 0.070	3.405 0.023	3.420	3.500 0.140	143	3.424 0.075
25	800125 0629	5	69	2.783 0.075	2.774 0.024	2.816	2.900 0.030	111	2.800 0.086
26	800127 0233	5	80	5.565 0.128	5.562 0.036	5.557	5.600 0.000	174	5.590 0.144
27	800413 0615	2	73	4.756 0.073	4.748 0.028	4.759	4.800 0.000	149	4.777 0.086
28	800413 0620	2	73	3.215 0.072	3.214 0.023	3.241	3.200 0.030	127	3.245 0.074
29	800413 1518	2	67	2.430 0.042	2.434 0.016	2.448	2.300 0.030	92	2.477 0.051
30	800413 2151	2	67	2.764 0.041	2.773 0.015	2.769	2.700 0.030	106	2.790 0.052
31	800413 2308	2	62	3.253 0.058	3.251 0.018	3.250	3.200 0.030	112	3.285 0.061
32	800419 1245	2	71	3.012 0.060	3.020 0.021	3.032	3.000 0.050	132	3.052 0.067
33	800421 1935	1	10	1.025 0.081	1.029 0.101	1.109	0.910 0.030	11	1.015 0.117
34	800428 1821	2	69	3.291 0.073	3.299 0.021	3.272	3.300 0.020	119	3.334 0.079
35	800510 2230	2	67	2.774 0.070	2.778 0.023	2.753	2.700 0.050	110	2.809 0.068
36	800519 0303	1	29	3.349 0.097	3.375 0.049	3.370	3.200 0.020	90	3.354 0.070
37	800612 0927	1	34	2.597 0.066	2.604 0.028	2.606	2.540 0.010	64	2.577 0.073
38	800613 0956	3	72	2.660 0.111	2.660 0.035	2.586	2.800 0.050	106	2.651 0.126
39	800618 0452	2	68	4.085 0.111	4.092 0.042	4.068	4.000 0.040	145	4.092 0.133
40	810117 0009	1	32	3.454 0.094	3.441 0.041	3.412	3.300 0.030	92	3.433 0.086
41	810127 2210	2	63	3.987 0.129	4.004 0.041	3.934	3.900 0.040	109	3.996 0.126
42	810325 1658	5	62	3.023 0.071	3.019 0.028	3.020	2.900 0.100	128	3.054 0.077
43	810411 2347	5	46	3.226 0.061	3.230 0.026	3.236	3.500 0.080	114	3.258 0.072
44	810523 0026	2	66	1.863 0.138	1.866 0.038	1.775	1.910 0.040	81	1.890 0.143
45	810523 1622	2	37	1.475 0.132	1.497 0.062	1.421	1.500 0.060	40	1.515 0.141
46	810527 1526	3	69	2.108 0.083	2.107 0.030	2.105	2.100 0.070	87	2.135 0.098
47	810528 0013	5	3	1.049 0.205	1.076 0.613	1.000	0.790 0.080	3	1.068 0.186
48	810530 1422	5	9	1.306 0.239	1.284 0.214	1.138	1.500 0.030	9	1.306 0.244
49	810530 1817	5	38	1.925 0.102	1.926 0.040	1.872	2.100 0.340	42	1.943 0.067
50	810603 1451	3	69	2.495 0.092	2.486 0.026	2.515	2.450 0.040	98	2.514 0.088
51	810603 1504	3	69	2.268 0.085	2.275 0.029	2.308	2.150 0.060	91	2.299 0.111
52	810606 0731	3	36	1.463 0.109	1.479 0.054	1.474	1.310 0.060	39	1.495 0.115
53	810606 1541	3	20	1.197 0.108	1.248 0.081	1.148	1.030 0.110	21	1.210 0.113
54	810612 0016	2	65	2.221 0.084	2.208 0.027	2.218	2.100 0.040	84	2.251 0.094
55	811120 0653	3	55	1.856 0.122	1.846 0.046	1.838	1.990 0.050	68	1.864 0.150
			3099	($t_p \leq 17.5$ sec)				5130	(all t_p)

Table 3. Site corrections. An asterisk indicates that the estimate for this station comes from earthquakes at distances greater than the P-wave travel-time of $t_P \geq 17.5$ sec. Stations denoted with asterisks or those with fewer than 5 observations are suspect, and should be used with caution. A standard error listed as a question mark indicates that the quantity is undefined because this station is represented by only 1 observation.

	STA	$\bar{\delta}$	SE	# OBS
*	ABR	0.189	?	1
*	ARJ	0.096	?	1
	BAV	0.031	0.065	34
	BBG	-0.219	0.040	23
	BBN	-0.255	0.186	22
	BCG	-0.026	0.028	31
	BEH	-0.225	0.033	30
	BEM	-0.098	0.045	18
	BHR	-0.301	0.080	6
	BHS	0.021	0.099	33
	BJC	0.157	0.061	33
	BJO	0.010	0.065	26
	BLR	-0.309	0.037	29
	BMC	0.091	0.035	30
	BMH	0.188	0.066	30
	BMS	-0.068	0.044	31
	BPC	-0.010	0.065	32
	BPF	0.105	0.105	28
	BPI	0.009	0.041	17
	BPP	-0.102	0.145	20
	BRM	-0.146	0.064	25
	BRV	-0.122	0.044	15
	BSB	-0.491	0.047	21
	BSC	-0.006	0.039	30
	BSG	0.231	0.105	29
	BSL	-0.682	0.104	17
	BSR	0.027	0.038	33
	BVL	-0.395	0.049	32
	BVY	-0.201	0.040	32
	CAC	-0.130	0.065	12
	CAD	0.245	0.071	27
	CAI	0.175	0.056	11
	CAL	0.079	0.044	40
	CAO	0.003	0.043	46
	CBR	0.243	0.040	13
	CBW	-0.054	0.079	11
	CCN	-0.137	0.061	12
	CCO	0.058	0.038	43
	CCY	0.357	0.062	35
	CDO	-0.190	0.100	23
	CDS	-0.202	0.112	11
	CDU	-0.209	0.097	9
	CDV	0.005	?	1
	CLC	-0.106	0.087	25
	CMC	0.209	0.071	13
	CMH	0.220	0.040	41
	CMJ	0.104	0.049	20
	CMM	0.256	0.054	22
	CMO	0.271	0.175	19
	CMP	0.228	0.049	23
	CMR	0.293	0.223	28
	CPL	0.188	0.048	33
	CRA	-0.202	0.040	14
	CRP	0.012	0.062	14
	CSC	-0.160	0.070	40
	CSH	0.239	0.065	36
	CTL	-0.120	0.052	14
	CVL	-0.245	?	1
*	GAF	0.407	0.192	6
*	GAX	0.228	0.079	14
*	GBD	0.240	0.182	4
*	GBG	-0.013	0.027	16
*	GBO	0.183	0.158	5
*	GCB	0.384	0.198	4

*	GCM	0.075	0.070	15
*	GCR	0.234	0.561	2
*	GCV	0.009	0.068	2
*	GCW	0.122	0.068	6
*	GDC	0.122	0.135	7
*	GFT	0.155	0.201	4
*	GGL	0.081	0.153	12
*	GGP	-0.143	0.077	18
*	GHC	-0.123	0.153	8
*	GHG	0.178	0.234	7
*	GHL	0.077	0.265	12
*	GHM	-0.138	0.288	3
*	GMC	0.122	0.067	10
*	GMK	-0.154	0.117	7
*	GMO	-0.043	0.203	7
*	GPM	0.249	0.108	5
*	GRM	-0.183	?	1
*	GRT	0.064	0.323	2
*	GSG	-0.333	0.059	6
*	GSM	0.063	0.040	21
*	GSN	0.122	0.185	11
*	GSS	0.118	0.138	11
*	GWK	-0.152	0.170	6
*	GWR	0.164	0.210	5
	HAZ	-0.040	0.090	36
	HBT	0.041	0.038	35
	HCA	-0.008	0.045	41
	HCB	-0.100	0.036	39
	HCO	-0.436	0.086	25
	HCP	0.067	0.067	20
	HCR	0.131	0.030	41
	HCZ	-0.246	0.087	23
	HDL	0.079	0.032	31
	HFE	0.102	0.059	43
	HFH	-0.631	0.062	32
	HFP	0.340	0.040	32
	HGS	0.233	0.053	27
	HGW	0.313	0.042	44
	HJG	0.189	0.040	37
	HJS	-0.087	0.047	32
	HKR	-0.631	0.095	31
	HLT	-0.004	0.053	32
	HMO	0.302	0.046	28
	HOR	-0.587	0.050	40
	HPH	-0.324	0.085	27
	HPL	0.456	0.062	40
	HPR	-0.403	0.081	25
	HQR	0.017	0.055	35
	HSF	-0.430	0.096	33
	HSL	-0.064	0.152	24
	JAL	0.238	0.043	41
	JBC	-0.026	0.029	37
	JBG	-0.307	0.049	37
	JBL	0.339	0.037	37
	JBM	0.125	0.036	40
	JBZ	-0.374	0.113	11
	JCB	-0.062	0.026	43
	JEC	-0.158	0.052	38
	JEG	0.257	0.103	25
	JHL	0.218	0.137	8
	JHP	-0.244	0.089	7
	JLT	-0.094	0.072	38
	JLX	0.285	0.052	34
	JMG	0.314	0.142	15
	JPL	-0.283	0.047	21
	JPP	-0.213	0.038	33
	JPR	0.429	0.281	10
	JPS	0.018	0.046	34
	JRG	-0.258	0.123	13
	JRR	0.301	0.071	16
	JRX	0.562	0.070	6
	JSA	0.132	0.068	20
	JSC	0.229	0.052	15
	JSF	-0.053	0.039	36
	JSG	-0.102	0.044	37

	JSJ	-0.028	0.045	39
	JSM	-0.104	0.063	20
	JSS	0.176	0.115	9
	JST	0.196	0.042	43
	JTG	-0.296	0.050	35
	JUC	0.254	0.040	32
	JWS	-0.137	0.060	21
*	KBB	0.614	?	1
*	KBN	0.060	0.030	3
*	KBR	0.056	?	1
*	KBS	-0.268	?	1
*	KCP	0.188	?	1
*	KCT	0.086	?	1
*	KFP	0.421	0.646	3
*	KGM	0.386	?	1
*	KMP	0.165	?	1
*	KRK	-0.107	?	1
*	LSL	0.118	?	1
*	MCU	0.164	0.054	10
*	MRF	1.064	?	1
	NBP	0.061	0.202	8
	NBR	-0.142	0.418	8
	NCD	-0.122	0.211	9
	NCF	-0.018	0.157	5
*	NDH	-0.502	0.149	6
*	NFI	0.328	0.075	10
*	NFR	-0.007	0.066	22
	NGV	-0.068	0.273	9
*	NHB	-0.012	0.091	23
	NHM	-0.391	0.119	10
	NLH	-0.012	0.202	8
	NLN	-0.013	0.071	10
*	NMH	0.071	0.048	23
*	NMT	0.209	0.109	21
*	NMW	-0.058	0.065	20
	NMX	-0.150	0.153	8
	NOL	0.327	0.313	8
	NPR	0.225	0.207	4
	NSH	-0.059	0.154	5
	NSP	-0.179	0.092	11
	NTM	-0.188	0.062	7
*	NWR	0.195	0.103	14
*	OGO	-0.073	?	1
	PAD	-0.145	?	1
	PAG	-0.019	0.179	5
*	PAN	-0.390	0.126	13
	PAP	0.095	0.056	10
	PAR	0.074	0.120	4
	PBR	0.186	0.154	3
	PBW	-0.210	0.083	11
	PBY	0.109	0.304	3
	PCA	0.140	0.303	5
	PCG	0.329	?	1
	PCR	0.246	0.165	5
	PGH	0.392	0.155	5
*	PHA	-0.413	0.481	3
	PHC	-0.021	0.113	4
	PHG	-0.331	0.085	4
	PHR	-0.069	0.334	19
	PIV	-0.559	0.329	5
	PJL	-0.199	0.068	18
	PLO	-0.354	0.076	31
	PMC	-0.292	0.242	5
	PMG	0.042	0.224	7
	PMP	-0.161	0.072	13
	PPF	-0.297	0.075	5
	PPT	0.018	0.068	9
	PRC	0.008	0.101	11
	PSA	-0.398	0.093	5
	PSE	-0.128	0.225	5
	PSM	-0.026	0.095	7
	PTY	-0.001	0.167	7
	PWK	-0.246	0.158	6
*	WJP	-0.104	?	1
*	WKT	-0.023	?	1

Table 4. Magnitude estimates for earthquakes in the test set. Refer to Tables 1-5 in Bakun [1984] for the source parameters. Regions are the same as in Table 2.

EV	DATE	REG	#OBS	MEDIAN+-MAD	MEAN+-95%	MODE	ML+-95%
61	770619 1424	5	5	1.508 0.068	1.550 0.317	1.500	1.230 0.110
62	770621 0444	5	6	1.408 0.141	1.415 0.222	1.400	1.490 0.090
64	770623 1822	5	6	1.638 0.064	1.689 0.142	1.757	1.960 0.100
65	780324 1942	3	15	2.492 0.066	2.480 0.078	2.471	2.500 0.050
66	780625 0801	1	5	1.820 0.039	1.792 0.153	1.866	1.580 0.000
67	780709 0518	1	5	1.309 0.144	1.303 0.205	1.159	1.190 0.190
69	780709 0520	2	5	1.212 0.084	1.155 0.225	1.266	1.120 0.000
70	781107 1300	1	25	2.631 0.102	2.673 0.060	2.638	2.600 0.040
71	781214 0715	3	6	1.352 0.023	1.416 0.161	1.328	1.220 0.050
72	790119 2115	2	46	2.806 0.053	2.799 0.029	2.839	2.700 0.100
73	790127 0052	2	17	2.729 0.074	2.696 0.064	2.627	2.600 0.180
74	790404 0749	2	24	2.952 0.076	2.941 0.052	2.967	3.000 0.050
75	790511 2252	2	45	2.791 0.121	2.809 0.042	2.922	2.800 0.100
76	790802 1416	2	33	2.699 0.076	2.721 0.033	2.670	2.900 0.040
77	790802 2041	2	22	3.527 0.059	3.537 0.051	3.507	3.100 0.050
78	790802 2052	2	25	3.096 0.079	3.105 0.039	3.111	2.600 0.050
79	790802 2143	2	19	4.178 0.086	4.176 0.057	4.149	3.900 0.040
80	790803 0242	4	25	2.802 0.074	2.780 0.040	2.809	2.800 0.040
81	790806 2221	4	31	3.457 0.083	3.470 0.045	3.456	3.400 0.030
83	790807 0512	4	13	1.588 0.115	1.554 0.092	1.603	1.970 0.050
84	790807 1415	4	17	2.220 0.078	2.217 0.077	2.263	2.260 0.070
85	790927 0614	2	5	2.871 0.014	2.824 0.202	2.869	2.900 0.030
86	791004 1859	1	7	0.877 0.055	0.990 0.186	0.932	0.760 0.060
87	791108 1806	2	24	2.791 0.100	2.762 0.060	2.844	2.540 0.060
88	791128 2251	2	15	2.638 0.088	2.633 0.067	2.674	2.500 0.030
89	791210 1411	2	21	2.944 0.049	2.948 0.030	2.935	2.700 0.040
91	800218 0810	2	14	2.745 0.115	2.728 0.083	2.724	2.400 0.040
93	800331 1016	3	22	2.708 0.058	2.723 0.034	2.722	2.700 0.110
94	800408 1336	2	23	2.503 0.037	2.512 0.074	2.496	2.300 0.070
95	800413 0750	2	17	2.539 0.083	2.540 0.065	2.512	2.500 0.040
96	800413 0758	2	21	3.492 0.078	3.494 0.056	3.489	3.200 0.050
97	800413 1539	2	7	2.813 0.073	2.860 0.130	2.780	2.800 0.040
98	800413 1702	2	24	2.892 0.034	2.885 0.034	2.900	2.800 0.020
99	800414 0049	2	18	2.734 0.048	2.735 0.048	2.708	2.600 0.030
100	800414 0155	2	16	1.944 0.065	1.962 0.048	1.946	1.900 0.140
101	800414 0345	2	12	2.567 0.089	2.569 0.076	2.563	2.500 0.060
102	800520 1521	1	3	0.918 0.071	0.900 0.248	0.850	0.650 0.050
103	800521 1927	1	9	2.311 0.122	2.346 0.119	2.200	2.200 0.040
104	800522 0440	1	4	1.327 0.121	1.418 0.502	1.300	0.980 0.010
105	800523 0910	1	3	1.156 0.080	1.182 0.301	1.150	1.060 0.040
106	810211 0847	5	44	3.160 0.072	3.185 0.049	3.167	3.100 0.070
107	810506 0916	2	40	2.726 0.119	2.734 0.042	2.834	2.600 0.050
108	810524 0344	3	45	2.202 0.070	2.175 0.044	2.230	2.250 0.060
109	810529 1112	3	23	1.050 0.281	1.123 0.159	0.938	0.680 0.010
110	810531 1238	5	3	1.009 0.169	1.053 0.590	1.000	1.380 0.000
111	810531 1635	5	11	1.638 0.153	1.619 0.113	1.582	1.460 0.160
112	810601 1544	2	38	1.631 0.117	1.677 0.055	1.565	1.630 0.060
113	810614 0750	2	49	2.968 0.070	2.982 0.030	2.968	2.700 0.050
114	810614 0755	2	68	2.824 0.097	2.788 0.062	2.816	2.900 0.070
115	810615 1429	2	35	1.785 0.107	1.775 0.075	1.764	1.740 0.080
			1016	(all t_p)			

Figure 1. Epicenters and CALNET stations used in this study. The earthquakes occured between mid-1977 through 1981. The independent set of earthquakes are denoted by squares, the test set are denoted by circles, and stations are noted as triangles. Wood-Anderson magnitudes are taken from Bakun [1984a]. The insert shows the depth distribution in each of the 5 source regions.

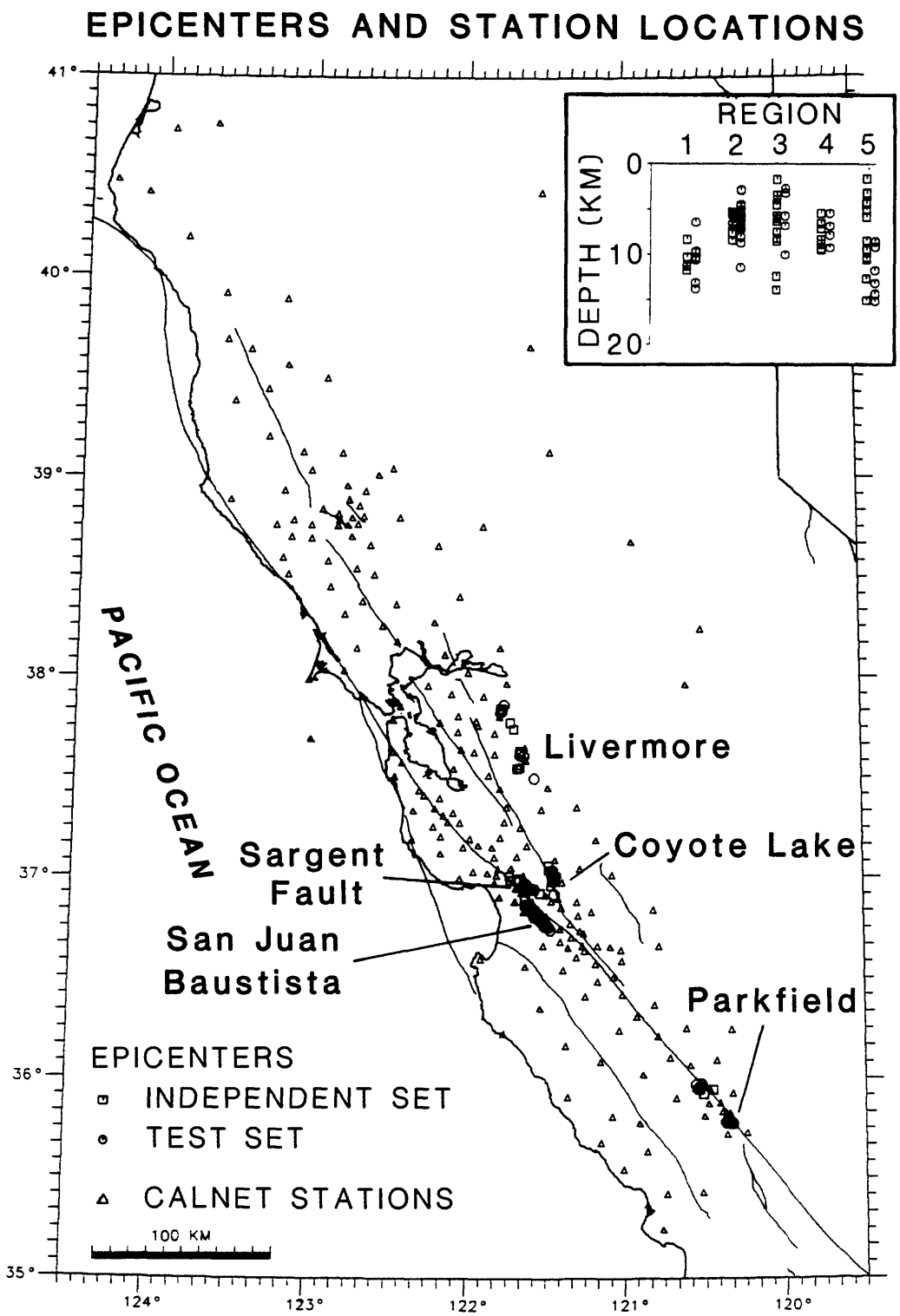

Figure 2. Log $\tilde{\tau}$ versus observed P-wave travel-time measured for the independent set of earthquakes. The solid curve represents the minimum $\tilde{\tau} = t_S$ criteria, where t_S is the expected S-wave travel-time. The symbol type indicates the source region (1) circle = Parkfield, (2) triangle = San Juan Bautista, (3) cross = Sargeant Fault, (4) X = Coyote Lake, and (5) diamond = Livermore, and are adopted in subsequent figures.

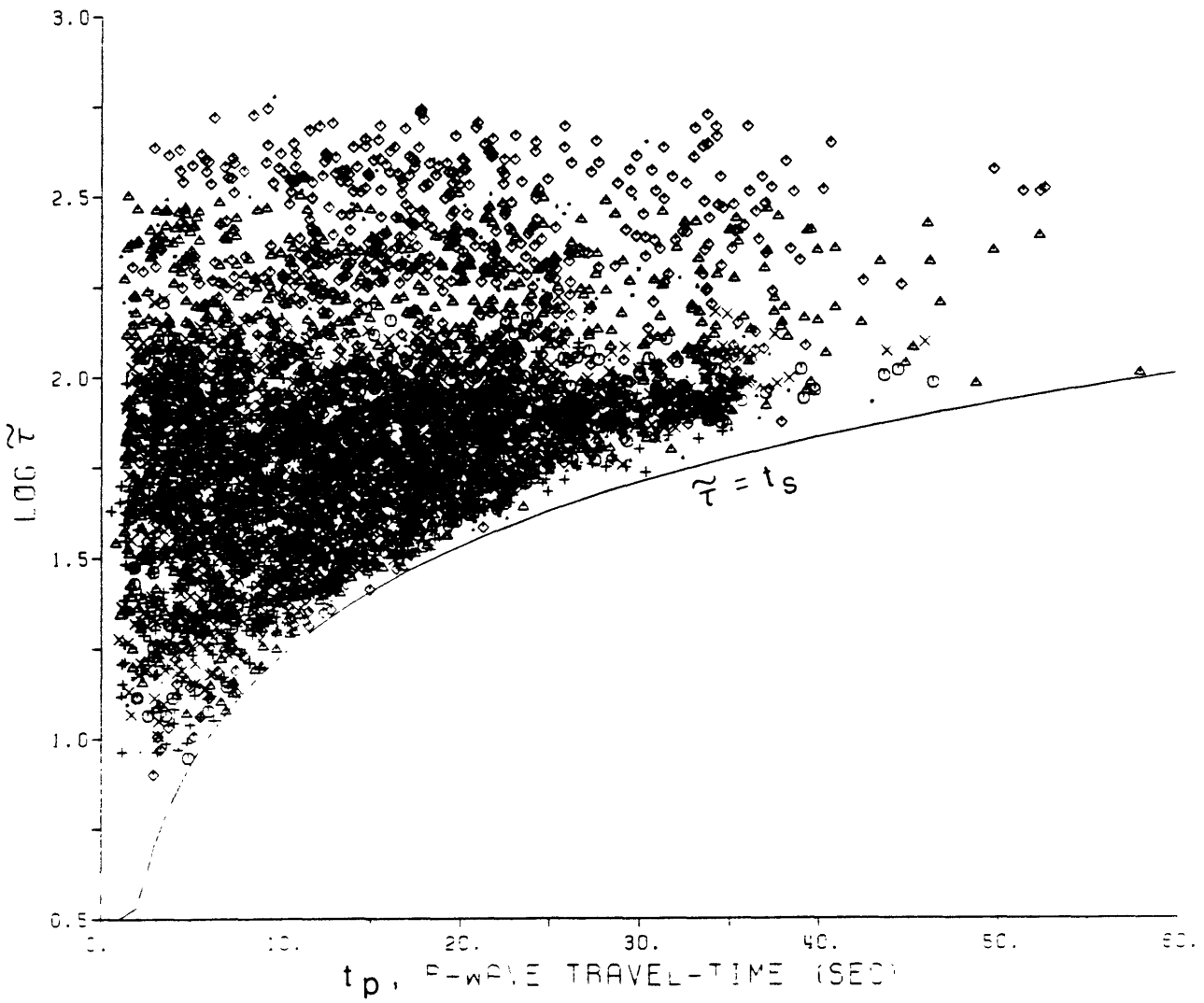

Figure 3. Signal amplitude as a function of time, in linear (top) and log space (bottom). Decreasing the instrument attenuation of the seismograph by 6 dB increases the signal amplitude by a factor of 2. The associated difference in duration of the signal is obtained through the relationship $\Delta \log t \sim -\frac{\Delta \log A}{q}$.

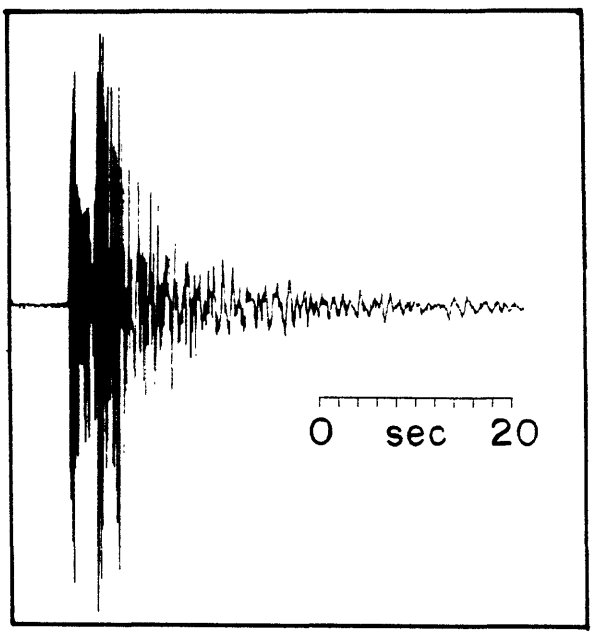

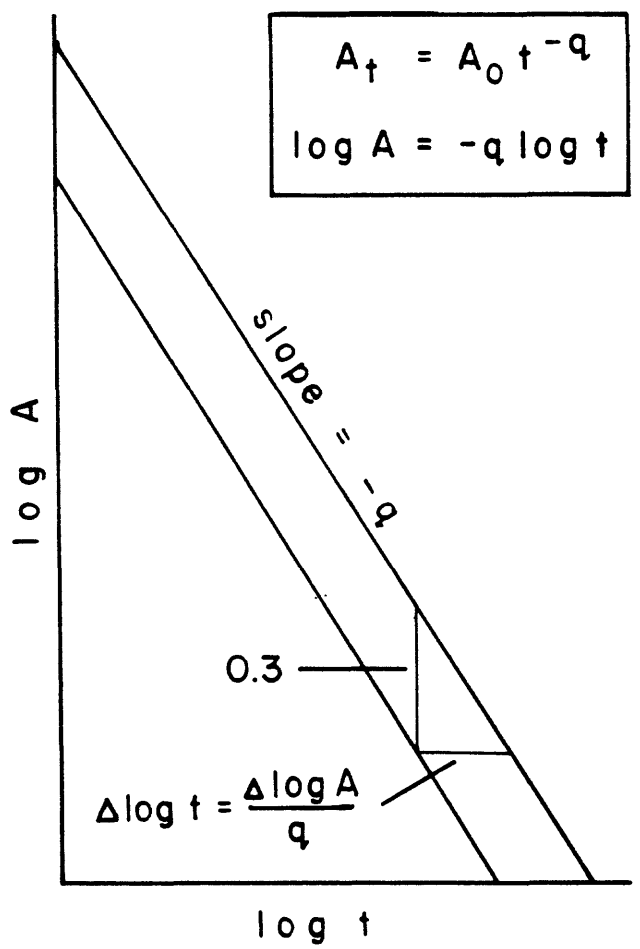

Figure 4. $\langle M_D \rangle$ versus Wood-Anderson and synthetic local magnitude $\overline{M}_L$ for the 55 earthquakes in the *independent set*. Vertical and horizontal bars represent the median absolute deviation *MAD*, and the 95% confidence limits of $\langle M_D \rangle$ and $\hat{M}_L$ respectively. $\langle M_D \rangle$ for the 5 earthquakes with $\hat{M}_L \leq 1.5$ slightly overestimate $\hat{M}_L$, but the differences $\langle M_D \rangle - \overline{M}_L$ are well within the error estimate, *MAD*.

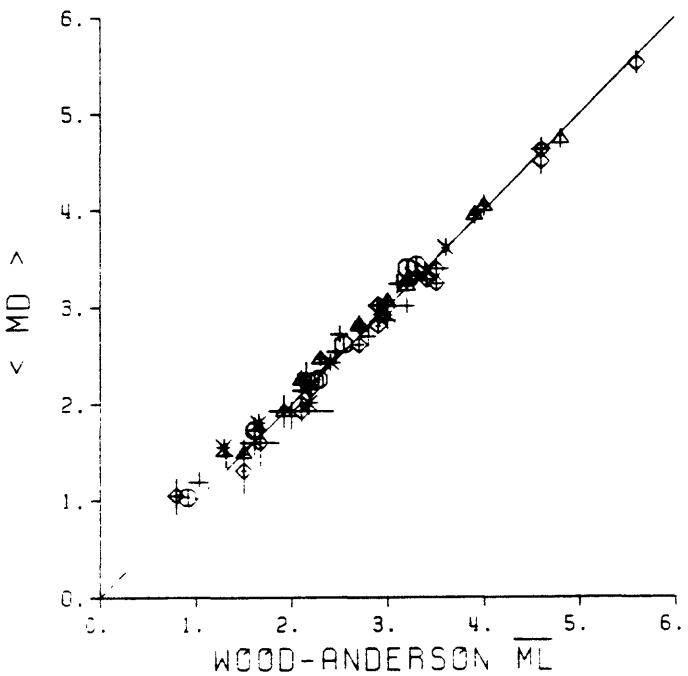

Figure 5. Magnitude misfit $\hat{\varepsilon}_{ij} = \hat{M}_{D_{ij}} - \langle M_D \rangle_i$ versus (a) log $\tilde{\tau}_{ij}$, (b) P-wave travel-time $t_{P_{ij}}$, (c) distance Δ_{ij}, and (d) azimuth. Symbol types are the same as in Figure 4. Large (small) symbols represent data that are within (exceed) ± *MAD* of that individual event.

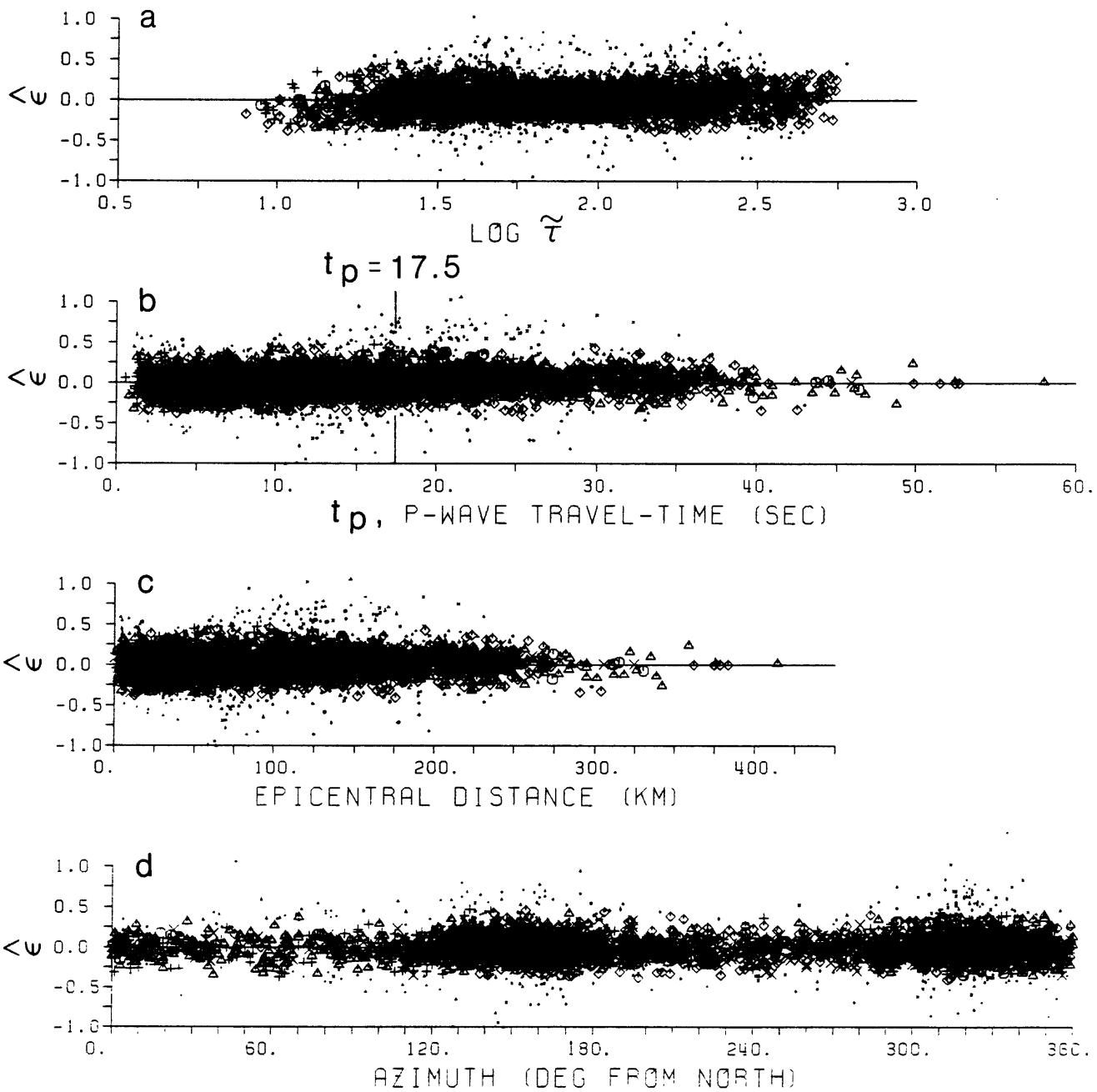

Figure 6. Magnitude misfit per event $\langle M_D \rangle_i - \overline{M}_{L_i}$ versus source depth. Symbols are the same as Figure 4.

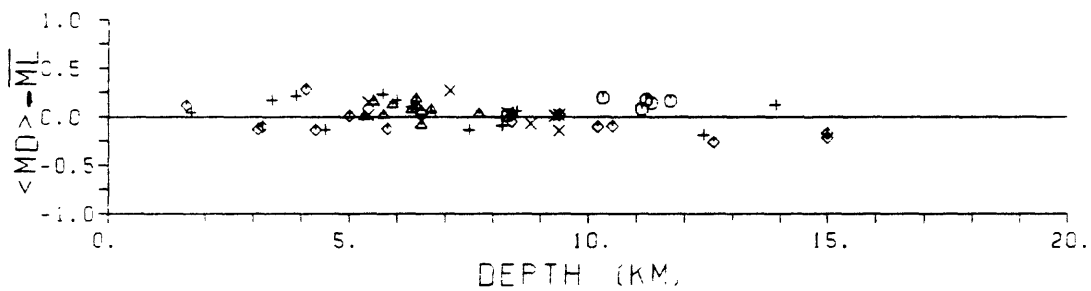

Figure 7. Top: Magnitude misfit $\hat{\varepsilon}_{ij}$ versus the instrument attenuation setting $attn_{ij}$ at the time of the i^{th} earthquake and at the j^{th} station. Bottom: Site correction $\overline{\delta}_j$ versus the average of the attenuation settings at the j^{th} station. (For example, if station XXX was set at 6 dB through 1980 and recorded 4 earthquakes in this time, but was then changed to 12 dB and recorded 2 earthquakes since 1981, then the average attenuation setting of station XXX for these 6 earthquakes is 8 dB.) Negative and positive corrections indicate sites that typically overestimate and underestimate earthquake magnitudes respectively.

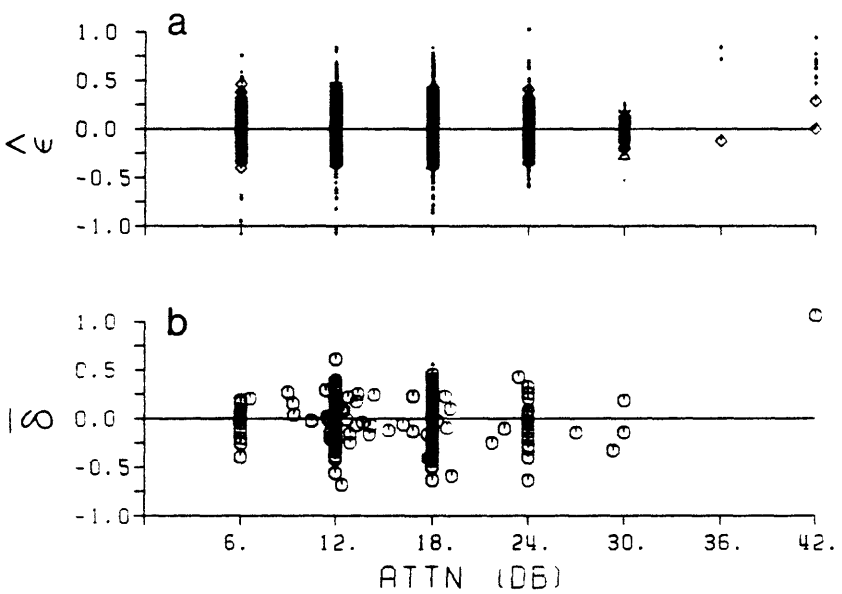

Figure 8. Site corrections $\bar{\delta}_j$ in map view. Negative corrections (open symbols) represent sites that typically overestimate earthquake magnitudes. Positive corrections (filled symbols) represent sites that typically underestimate earthquake magnitudes. The symbol size is proportional to the absolute value of the station correction, the larger symbols have greater corrections. Stations with standard errors less than 0.25 or that recorded more than 5 events are denoted as squares, all others are denoted as circles.

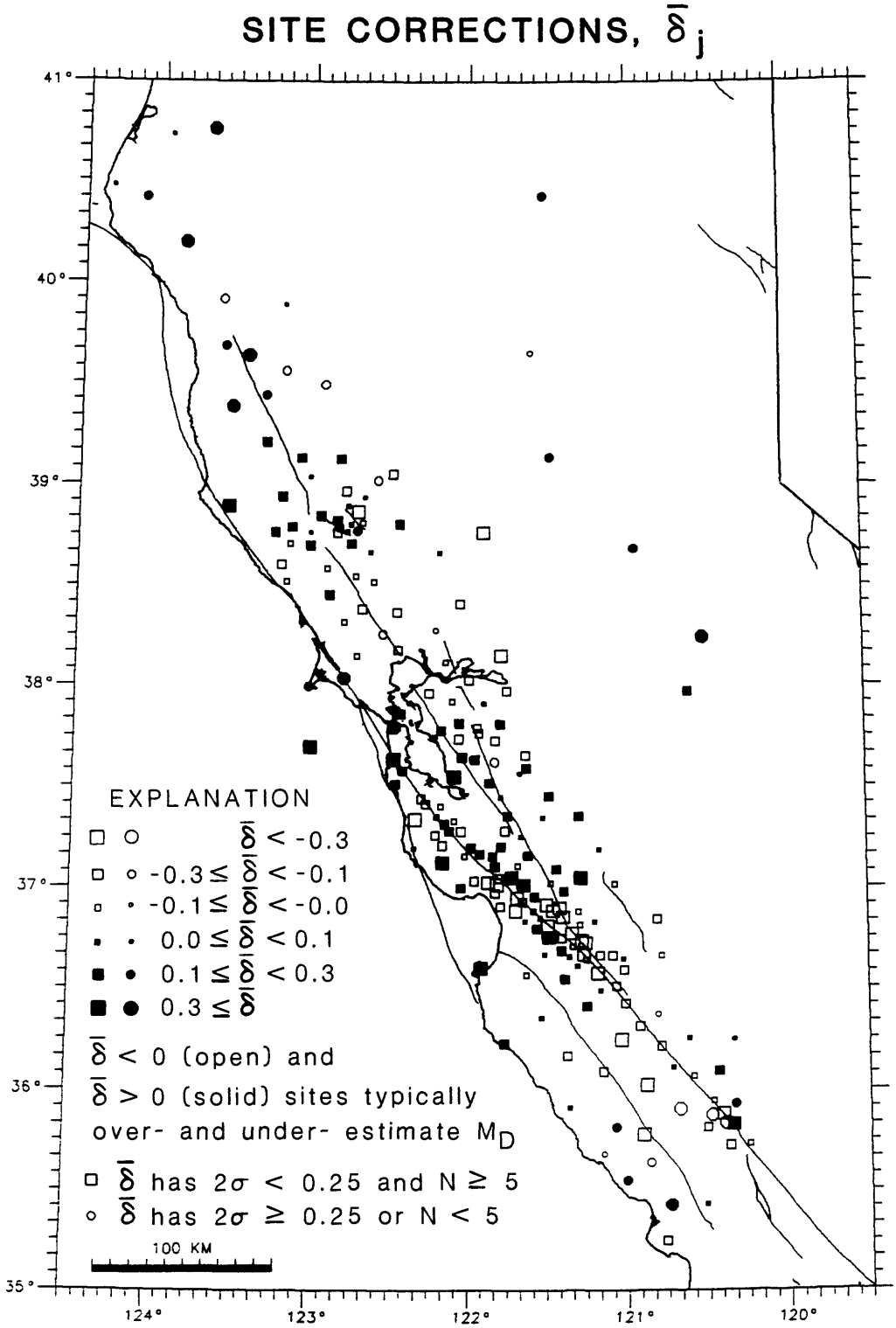

Figure 9. Top: Site corrections $\overline{\delta}_j$ versus geologic code of Evernden, *et. al* [1981]. A = granitic and metamorphic rocks; B = Paleozoic sediments; C = Early Mesozoic sediments; D = Cretaceous-Eocene sediments; E = Early Tertiary sediments; F = Oligocene-Pliocene sediments; J = Quaternary sediments; H = Tertiary volcanics; I = Quaternary volcanics; U = rocks of unknown affinities. Bottom: Site corrections $\overline{\delta}_j$ versus the isostatic residual gravity field in milligalls taken from Jachens and Griscom [1985]. Symbols refer to the geologic code in the top diagram.

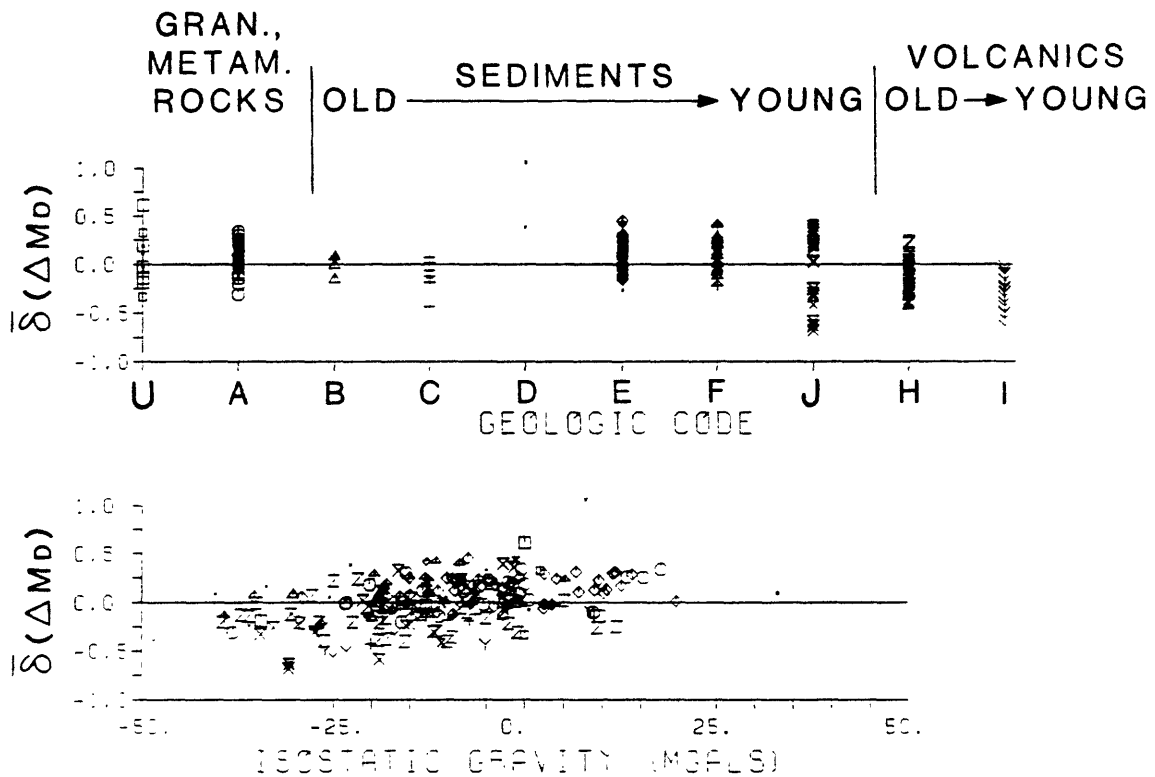

Figure 10. $<M_D>$ versus Wood-Anderson and synthetic local magnitude $\overline{M_L}$ for the *test set*. Symbols are the same as Figure 4.

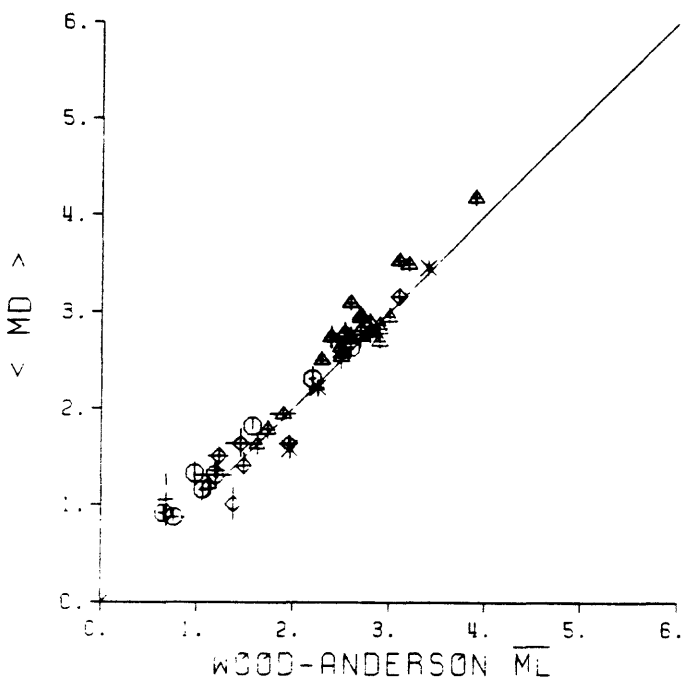

Figure 11. Magnitude misfit $\hat{\epsilon}_{ij} = \hat{M}_{D_{ij}} - \langle M_D \rangle_i$ for the test set versus (a) log $\tilde{\tau}_{ij}$, (b) P-wave travel-time $t_{P_{ij}}$, (c) azimuth and (d) depth. Symbols are the same as in Figure 4.

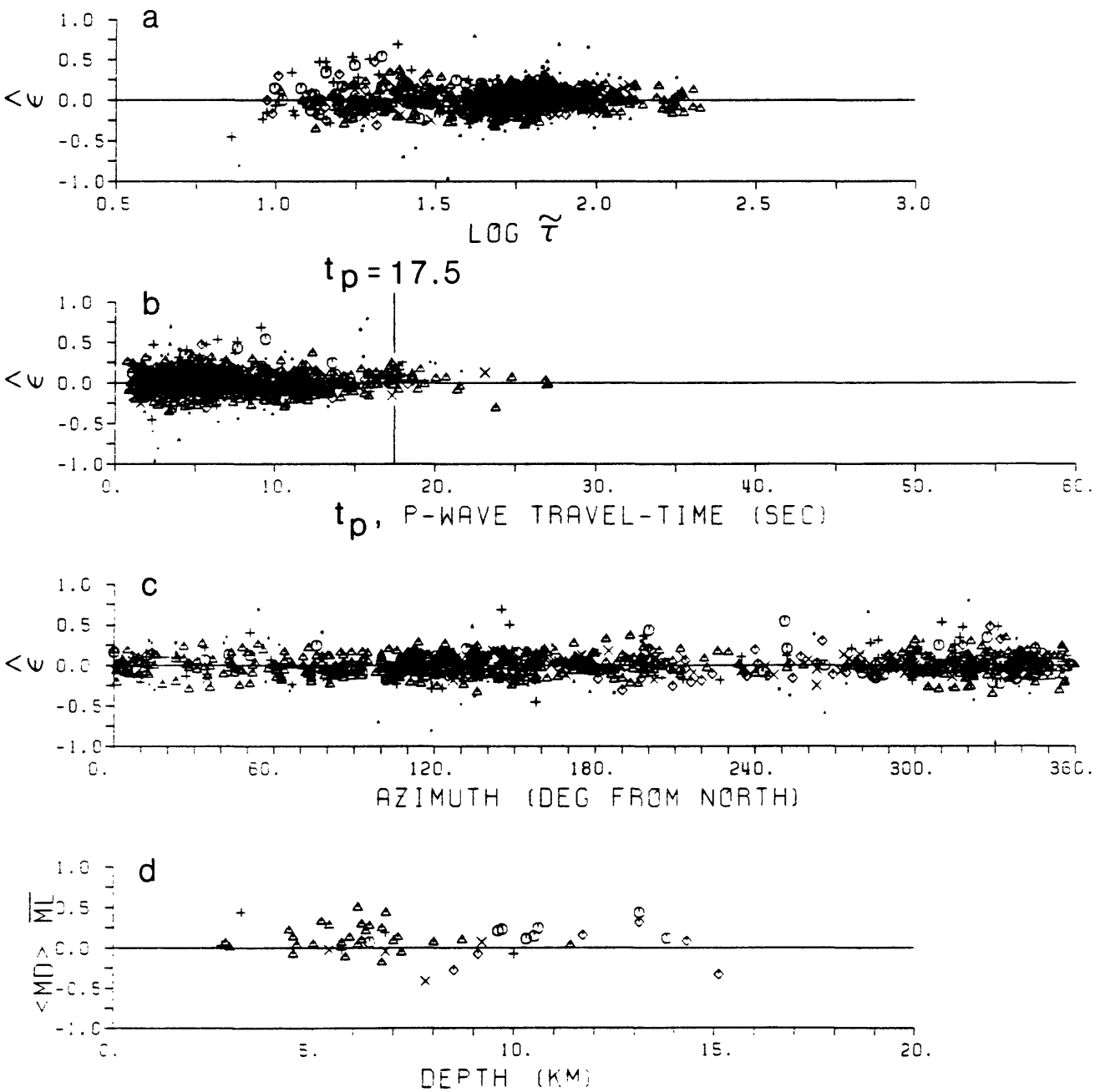

Appendix A. Frequency of magnitude estimates $\hat{M}_D$ for each earthquake in the independent set. $\hat{M}_L \pm 95\%$ confidence intervals obtained from Bakun [1984b] are plotted as inverted arrows and horizontal bars at the top of each histogram. Beneath $\hat{M}_L$ are plotted the 3 measures of central tendency and error of M_D calculated in this study: the mode, the median $<M_D> \pm MAD$, and the mean $\overline{M_D} \pm 95\%$ confidence intervals. The number of duration measurements, N, are also listed. The event numbers (same as in Table 2) are printed in the upper right corner of each diagram. The width of the M_D window is 0.2 if N is less than 30, otherwise 0.1 is set as the width of the window. The + symbols represents a weighted 3-point running average of the frequency distribution of M_D estimates used to estimate the mode.

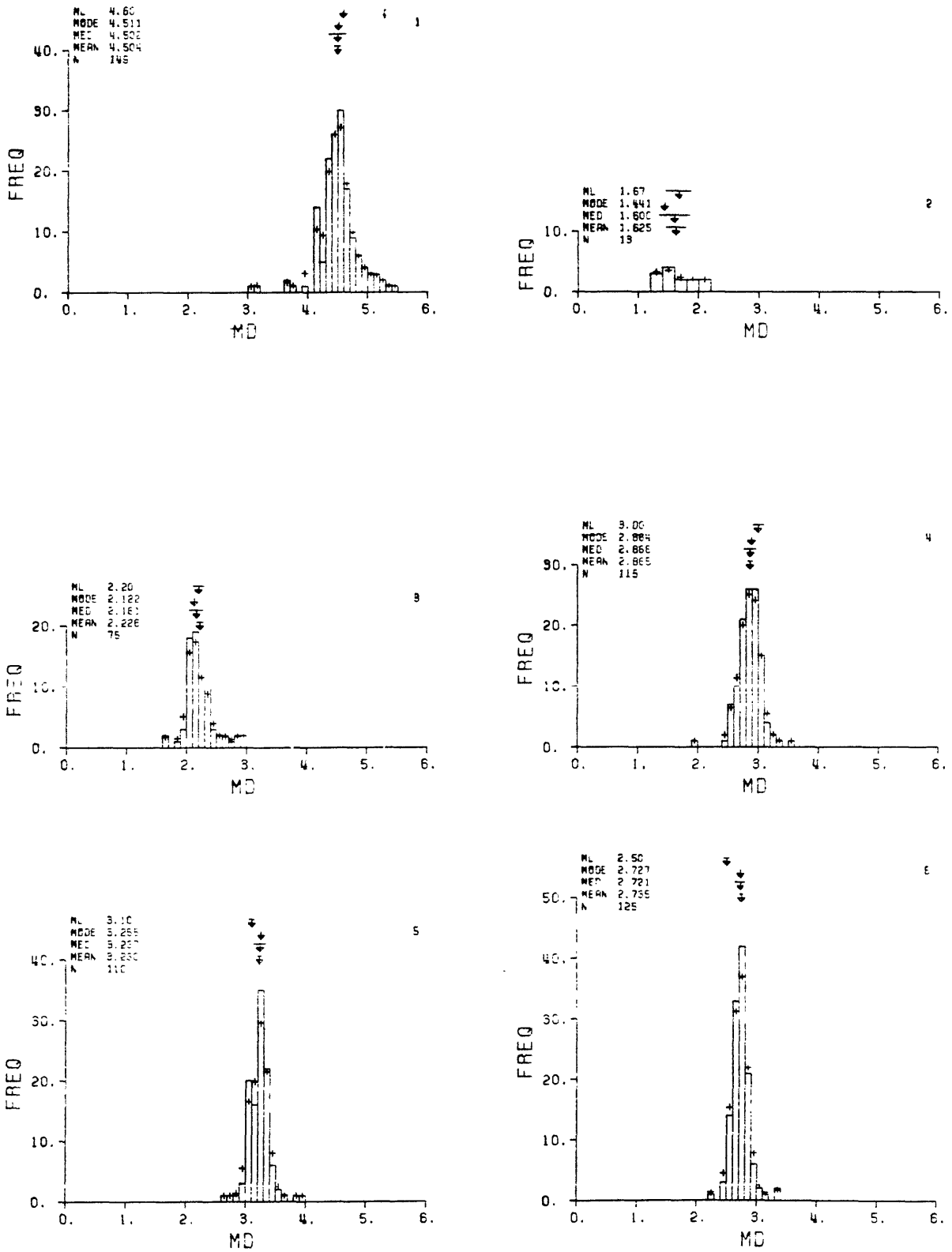

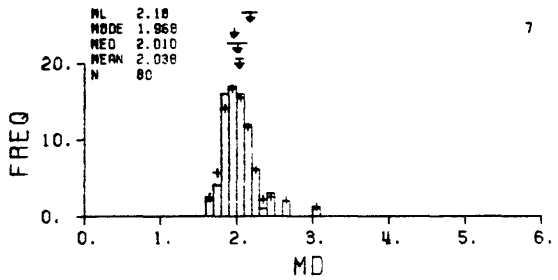
7
ML 2.18
MODE 1.968
MED 2.010
MEAN 2.038
N 80
FREQ
MD

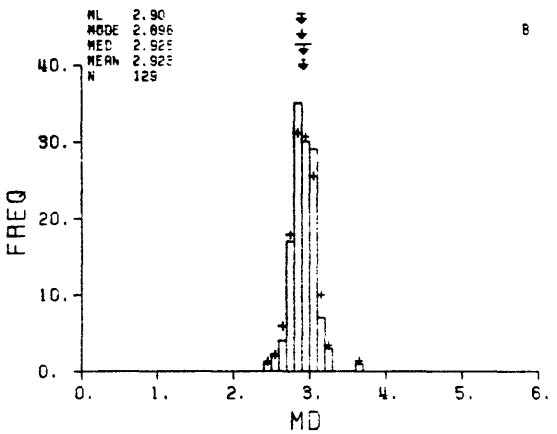
8
ML 2.90
MODE 2.896
MED 2.925
MEAN 2.923
N 129
FREQ
MD

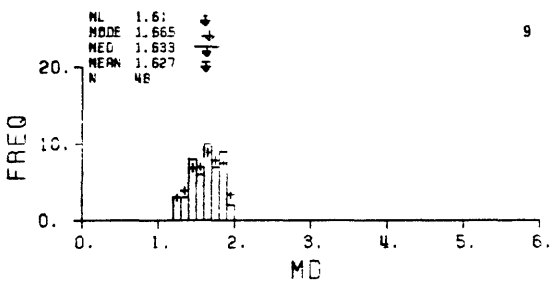
9
ML 1.61
MODE 1.665
MED 1.633
MEAN 1.627
N 46
FREQ
MD

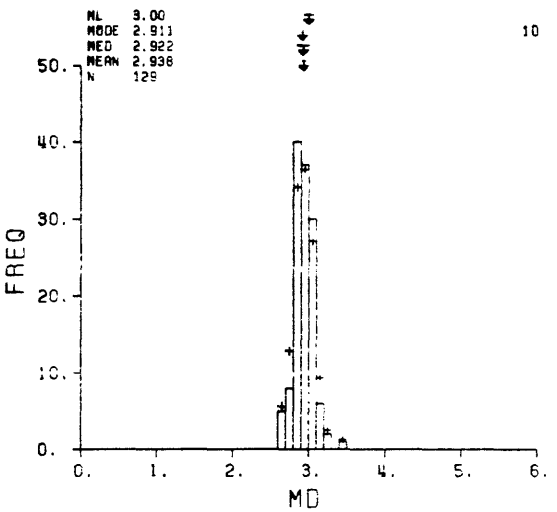
10
ML 3.00
MODE 2.911
MED 2.922
MEAN 2.938
N 129
FREQ
MD

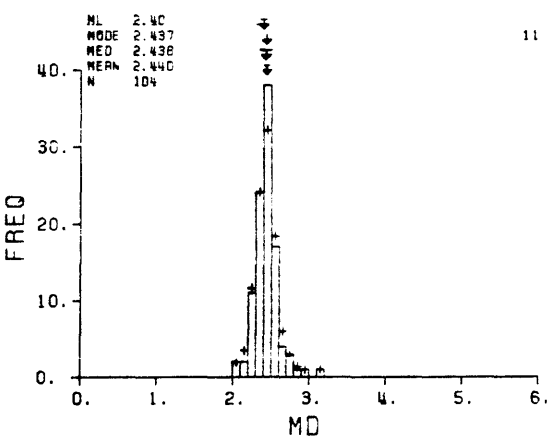
11
ML 2.40
MODE 2.437
MED 2.438
MEAN 2.440
N 104
FREQ
MD

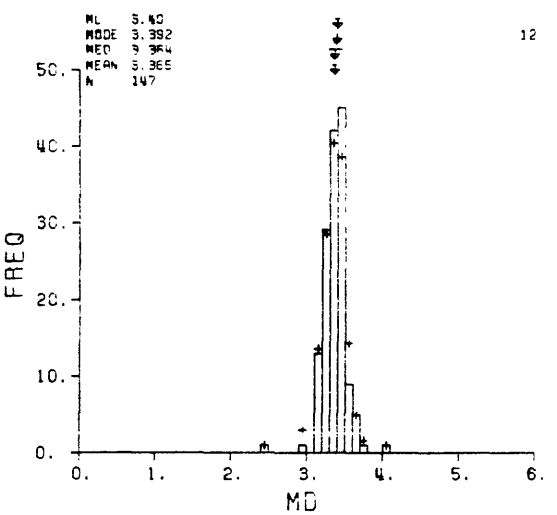
12
ML 5.40
MODE 5.392
MED 5.384
MEAN 5.365
N 147
FREQ
MD

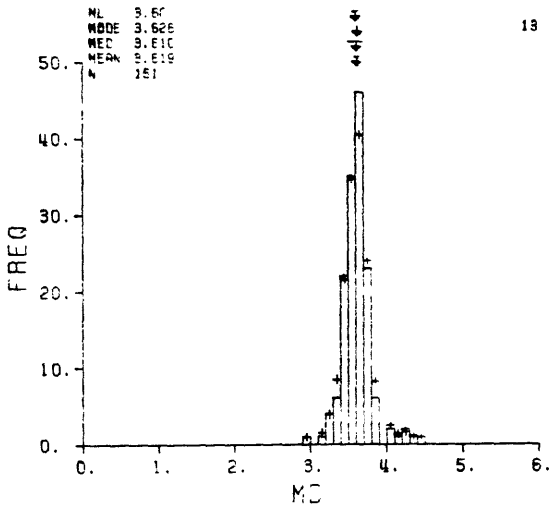
ML 3.67
MODE 3.628
MED 3.610
MEAN 3.619
N 151
13
FREQ
MD

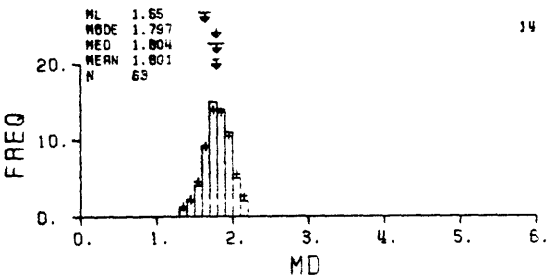
ML 1.85
MODE 1.797
MED 1.804
MEAN 1.801
N 69
14
FREQ
MD

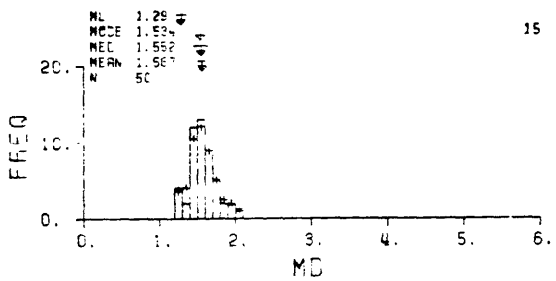
ML 1.29
MODE 1.534
MED 1.552
MEAN 1.567
N 50
15
FREQ
MD

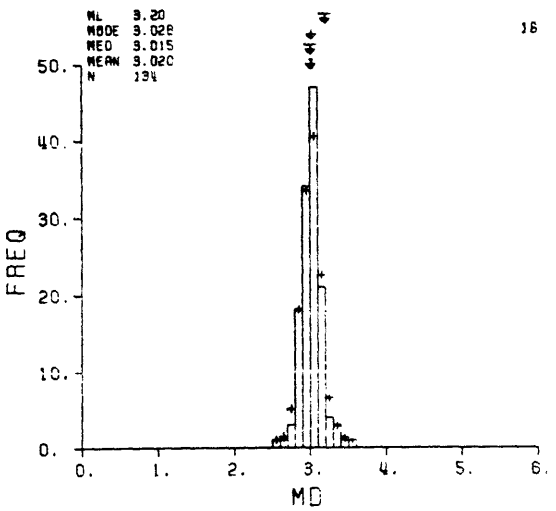
ML 3.20
MODE 3.028
MED 3.015
MEAN 3.020
N 134
16
FREQ
MD

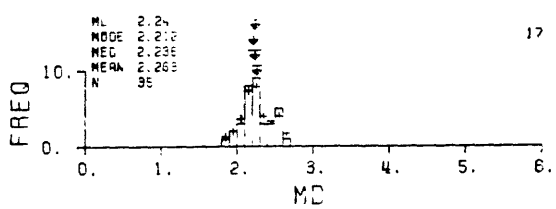
ML 2.24
MODE 2.210
MED 2.236
MEAN 2.268
N 95
17
FREQ
MD

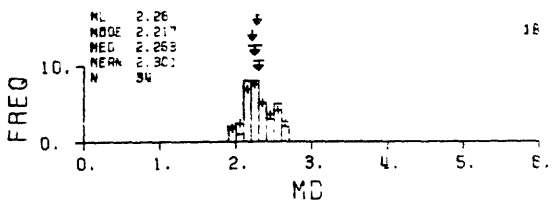
ML 2.26
MODE 2.217
MED 2.268
MEAN 2.301
N 94
18
FREQ
MD

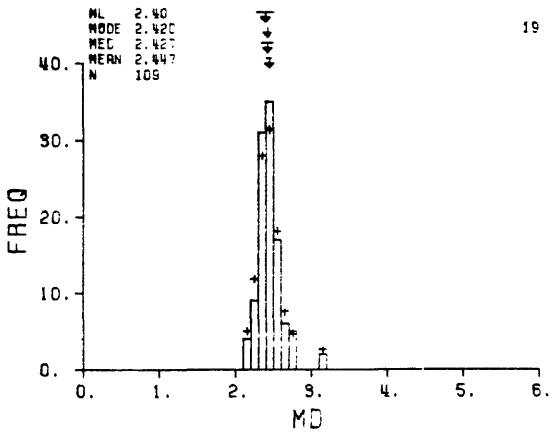
ML 2.40
MODE 2.420
MED 2.427
MEAN 2.447
N 109
19
FREQ
MD

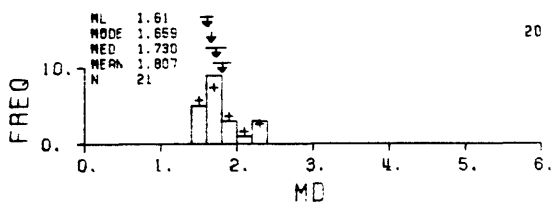
ML 1.61
MODE 1.669
MED 1.730
MEAN 1.807
N 21
20
FREQ
MD

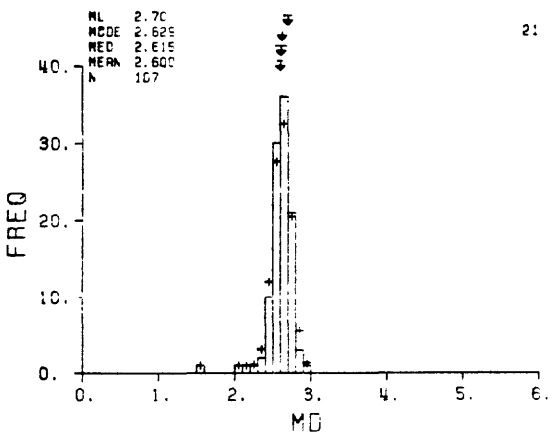
ML 2.70
MODE 2.629
MED 2.615
MEAN 2.600
N 107
21
FREQ
MD

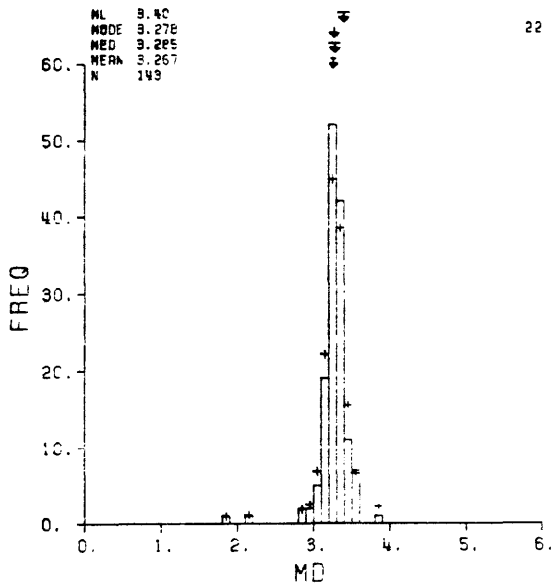
ML 3.40
MODE 3.278
MED 3.285
MEAN 3.267
N 149
22
FREQ
MD

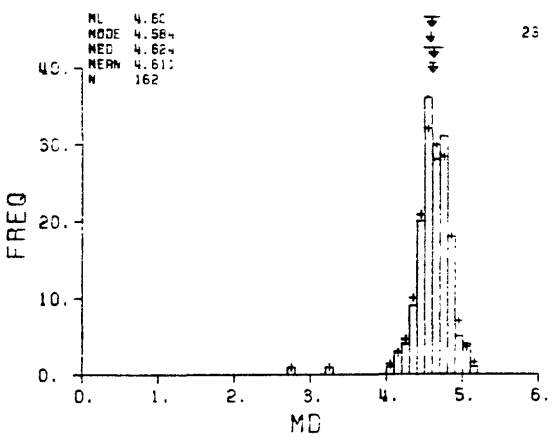
ML 4.60
MODE 4.584
MED 4.624
MEAN 4.611
N 162
23
FREQ
MD

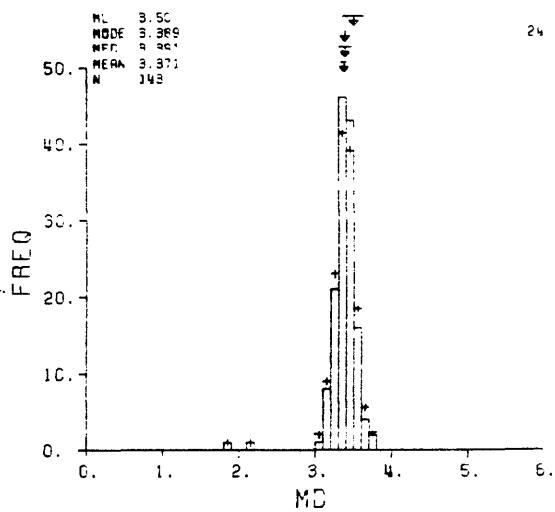
ML 3.50
MODE 3.369
MEAN 3.371
N 143
24
FREQ
MD

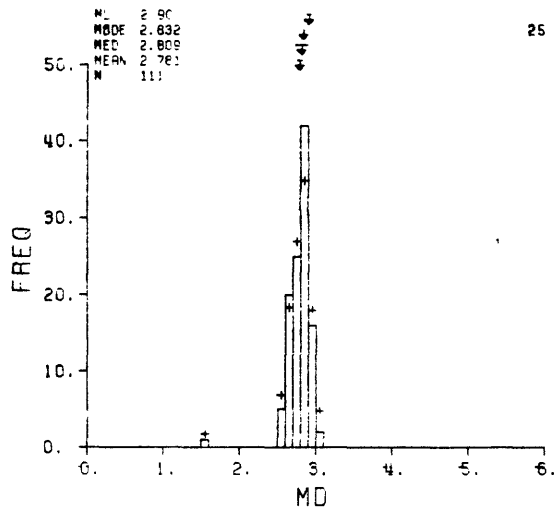
MODE 2.832
MED 2.809
N 111
25
FREQ
MD

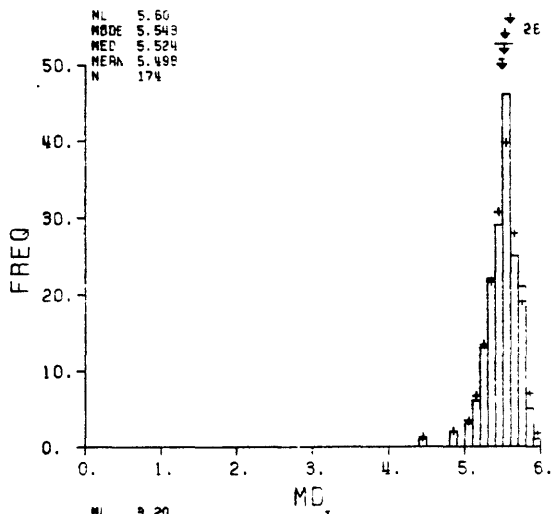
MODE 5.548
MED 5.524
MEAN 5.499
N 174
26
FREQ
MD

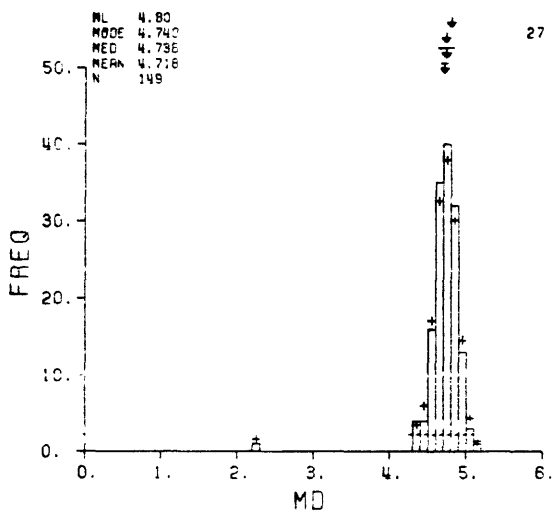
MODE 4.740
MED 4.736
MEAN 4.716
N 149
27
FREQ
MD

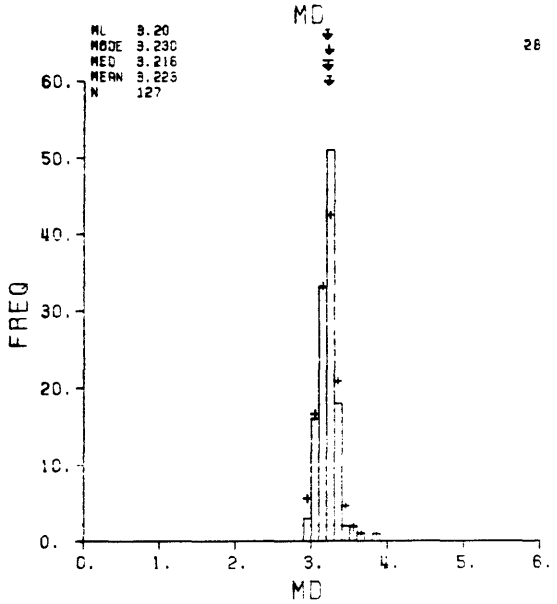
MODE 3.230
MED 3.216
MEAN 3.225
N 127
28
FREQ
MD

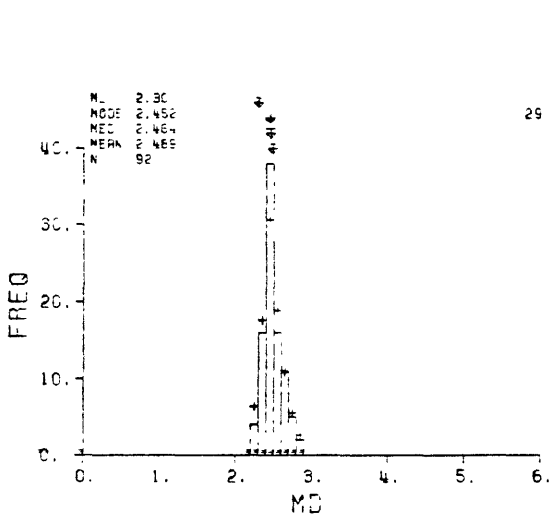
29
FREQ
MD

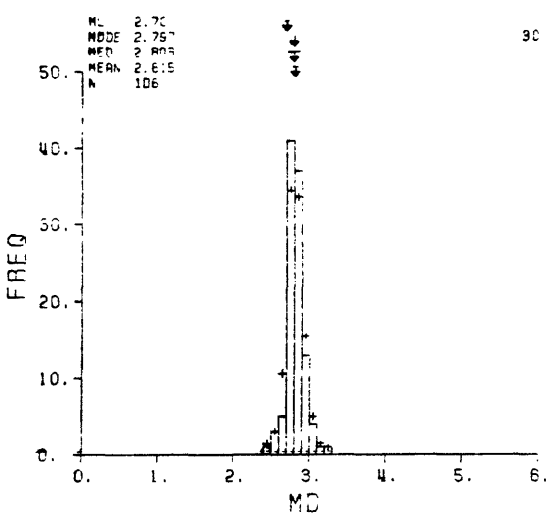
30
FREQ
MD

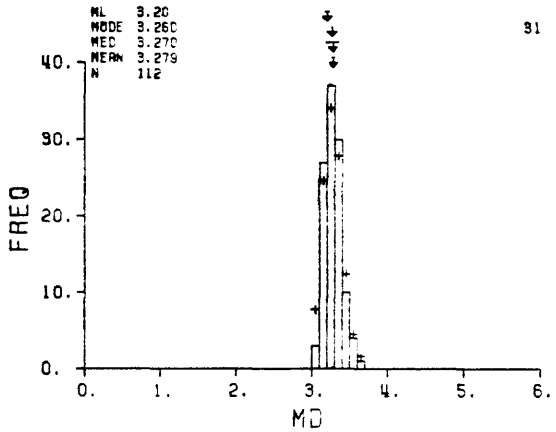
ML 3.20
MODE 3.260
MED 3.270
MEAN 3.279
N 112
91
FREQ
MD

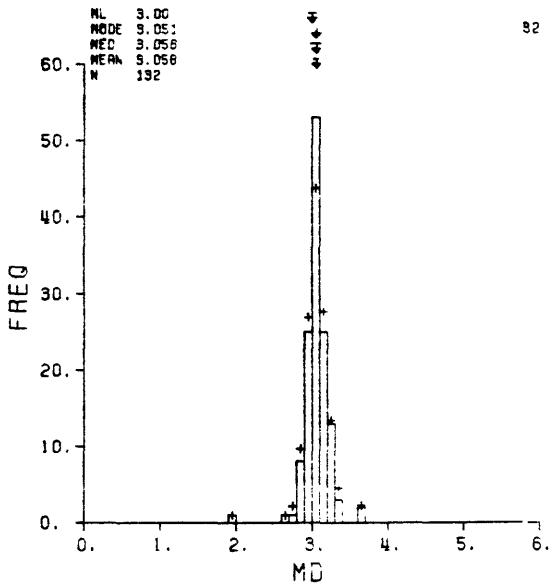
ML 3.00
MODE 3.051
MED 3.058
MEAN 3.058
N 192
92
FREQ
MD

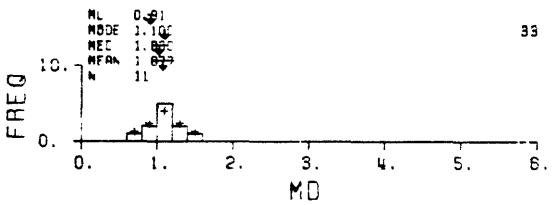
93
FREQ
MD

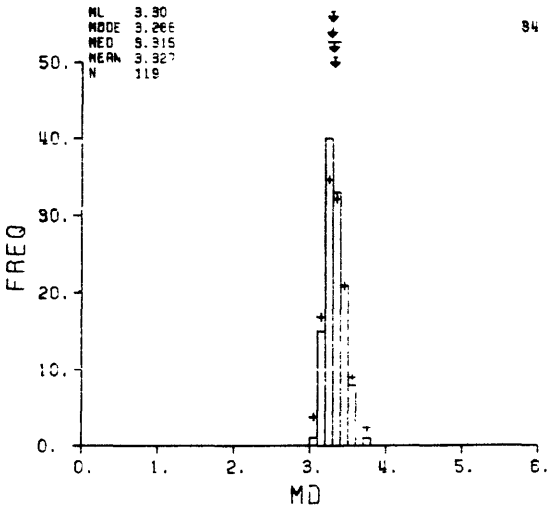
ML 3.30
MODE 3.266
MED 3.315
N 119
94
FREQ
MD

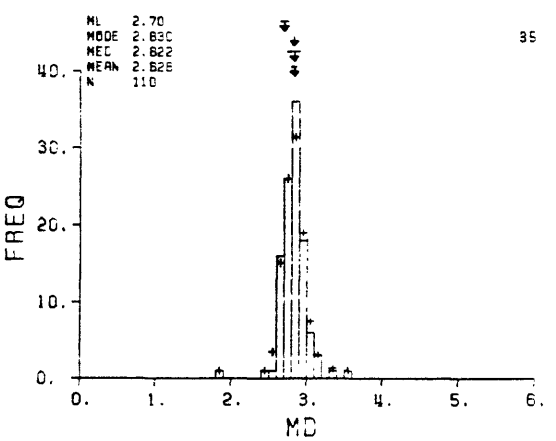
ML 2.70
MODE 2.690
MED 2.822
MEAN 2.828
N 110
95
FREQ
MD

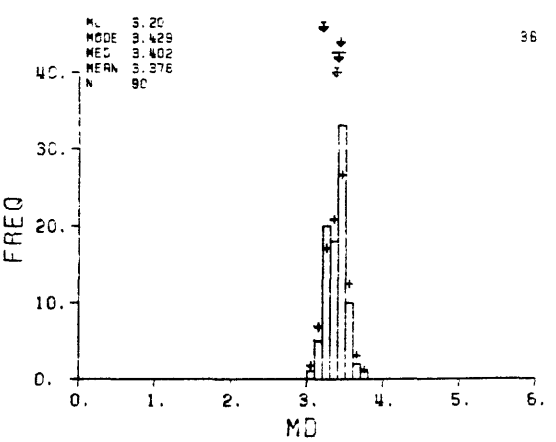
ML 3.20
MODE 3.429
MED 3.402
MEAN 3.378
N 90
96
FREQ
MD

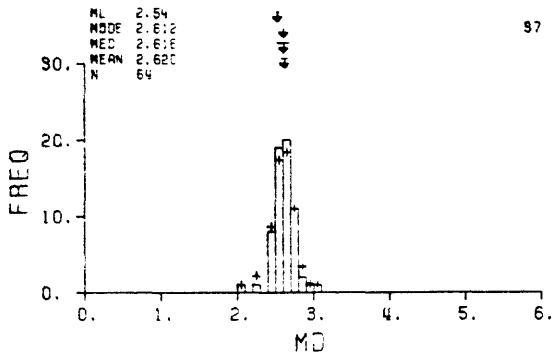
ML 2.54
MODE 2.612
MED 2.618
MEAN 2.620
N 64
37
FREQ
MD

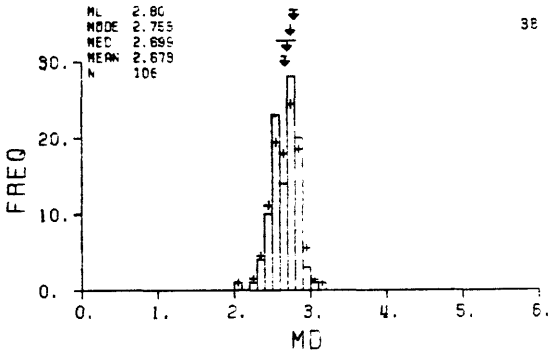
ML 2.80
MODE 2.755
MED 2.699
MEAN 2.679
N 106
38
FREQ
MD

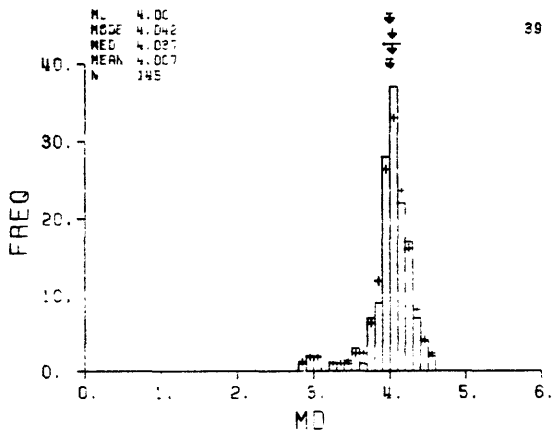
ML 4.00
MODE 4.042
MED 4.037
MEAN 4.007
N 145
39
FREQ
MD

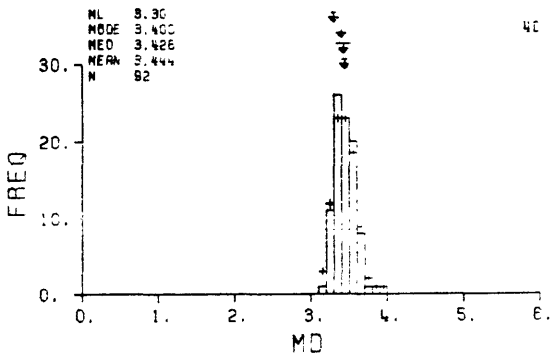
ML 3.30
MODE 3.400
MED 3.426
MEAN 3.444
N 92
40
FREQ
MD

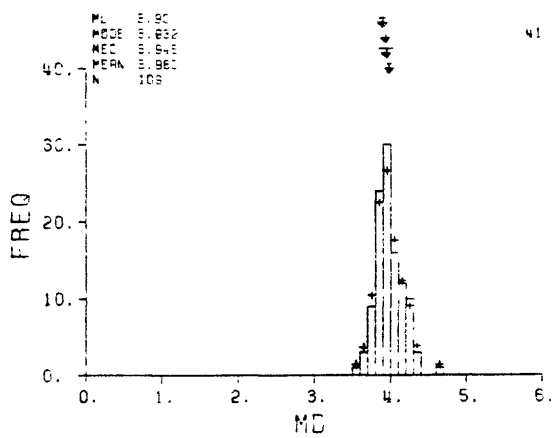
41
FREQ
MD

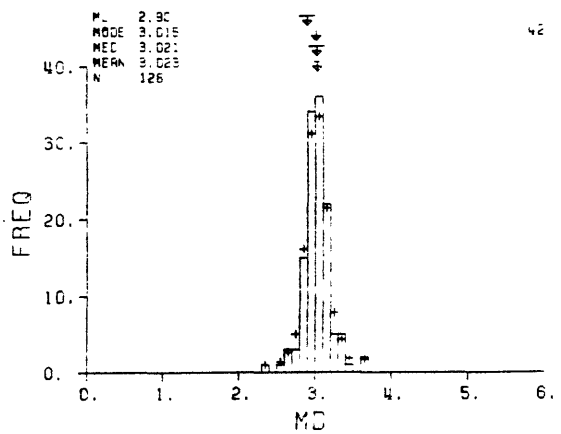
42
FREQ
MD

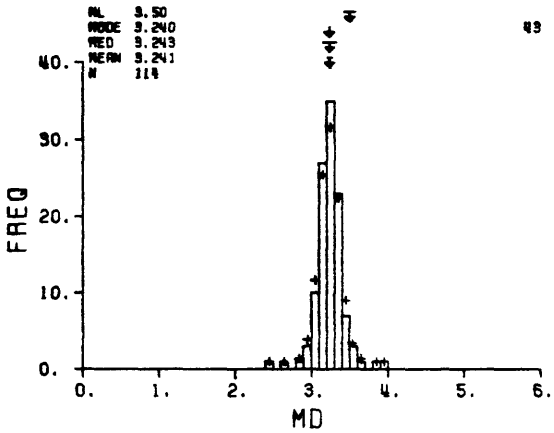
ML 3.50
MODE 3.240
MED 3.243
MEAN 3.241
N 114
43
FREQ
MD

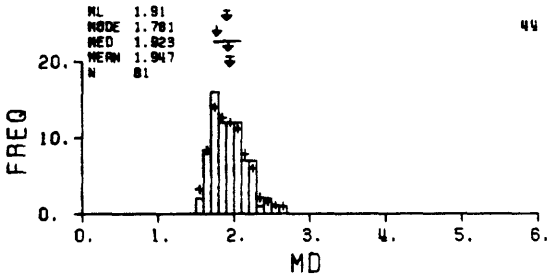
ML 1.91
MODE 1.781
MED 1.823
MEAN 1.947
N 81
44
FREQ
MD

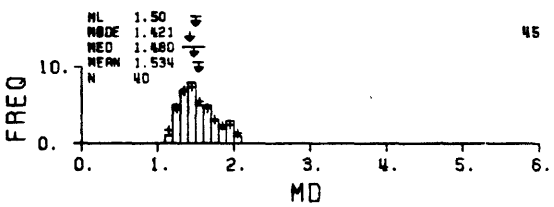
ML 1.50
MODE 1.421
MED 1.480
MEAN 1.534
N 40
45
FREQ
MD

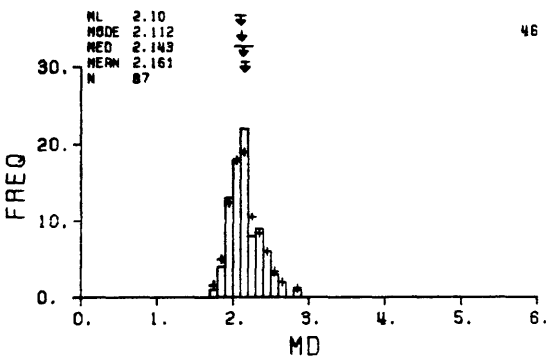
ML 2.10
MODE 2.112
MED 2.143
MEAN 2.161
N 87
46
FREQ
MD

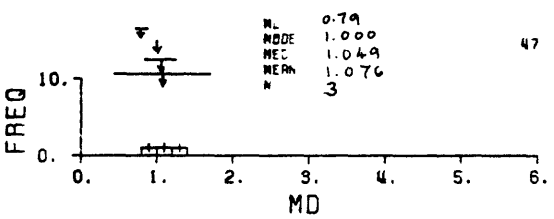
ML 0.79
MODE 1.000
MED 1.049
MEAN 1.076
N 3
47
FREQ
MD

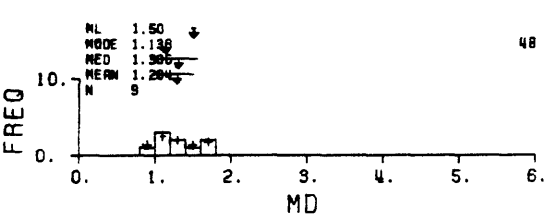
ML 1.50
MODE 1.138
MED 1.300
MEAN 1.284
N 9
48
FREQ
MD

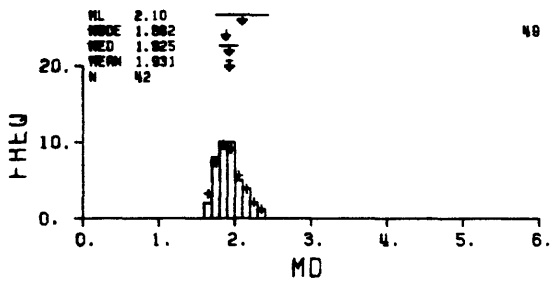
ML 2.10
MODE 1.882
MED 1.825
MEAN 1.891
N 42
48
FREQ
MD

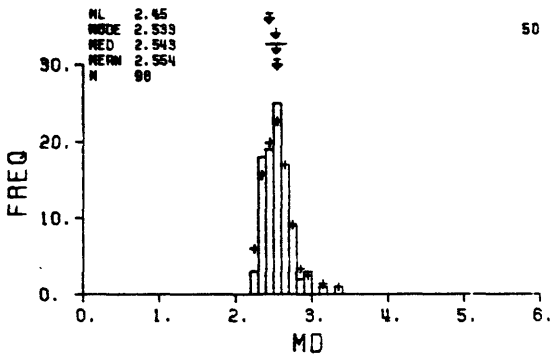
ML 2.45
MODE 2.539
MED 2.543
MEAN 2.554
N 98
50
FREQ
MD

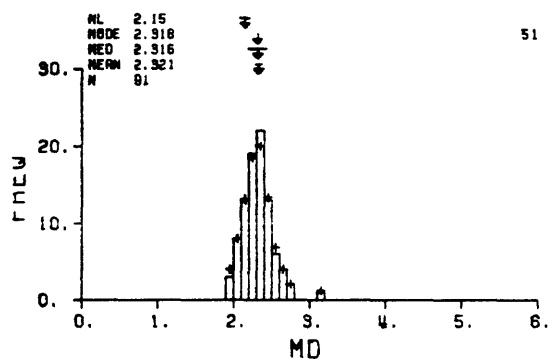
ML 2.15
MODE 2.918
MED 2.316
MEAN 2.321
N 81
51
FREQ
MD

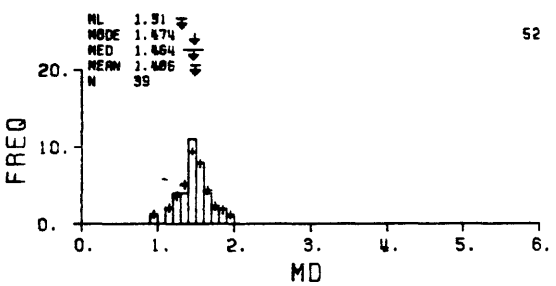
ML 1.91
MODE 1.474
MED 1.464
MEAN 1.486
N 99
52
FREQ
MD

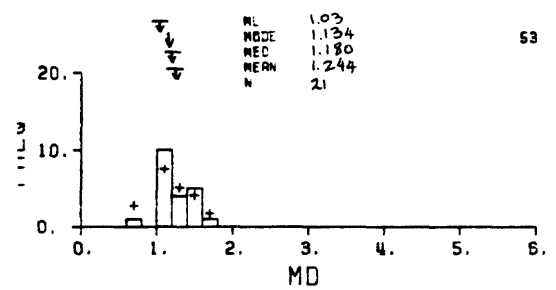
ML 1.03
MODE 1.134
MED 1.180
MEAN 1.244
N 21
53
MD

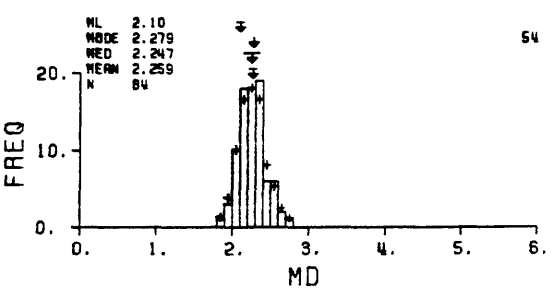
ML 2.10
MODE 2.279
MED 2.247
MEAN 2.259
N 84
54
FREQ
MD

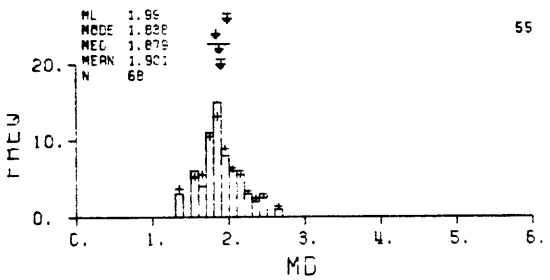
ML 1.99
MODE 1.888
MED 1.879
MEAN 1.901
N 68
55
20.
10.
0.
FREQ
0.
1.
2.
3.
4.
5.
6.
MD

Appendix B. Frequency of magnitude estimates $\hat{M}_D$ for each earthquake in the test set. The event numbers correspond to those in Table 4. See Appendix A for explanation of the diagrams.

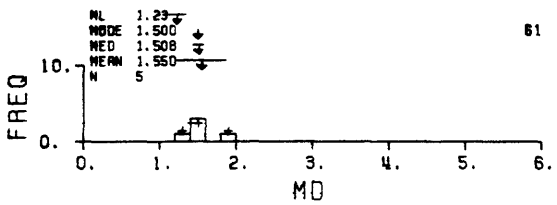

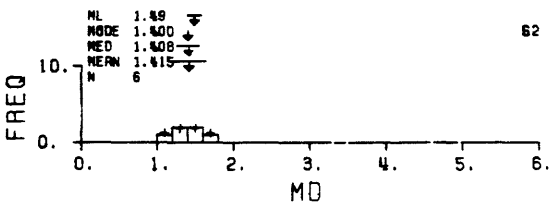

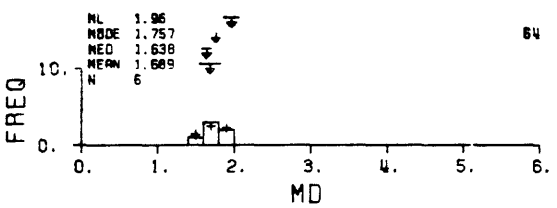

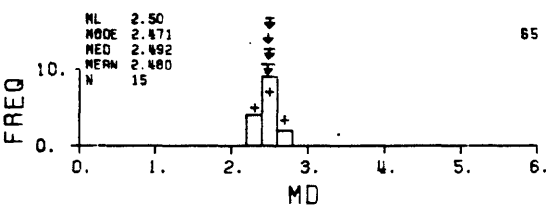

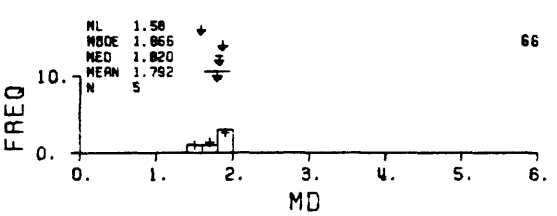

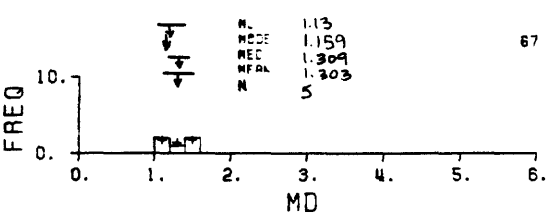

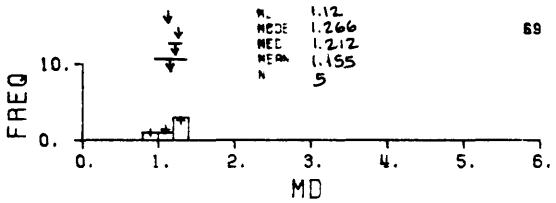
69
ML 1.12
MODE 1.266
MED 1.212
MEAN 1.155
N 5
FREQ
10.
0.
0. 1. 2. 3. 4. 5. 6.
MD

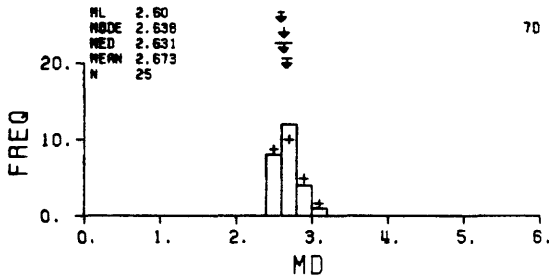
70
ML 2.60
MODE 2.638
MED 2.631
MEAN 2.673
N 25
FREQ
20.
10.
0.
0. 1. 2. 3. 4. 5. 6.
MD

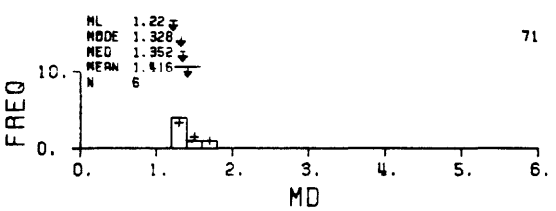
71
ML 1.22
MODE 1.328
MED 1.352
MEAN 1.416
N 6
FREQ
10.
0.
0. 1. 2. 3. 4. 5. 6.
MD

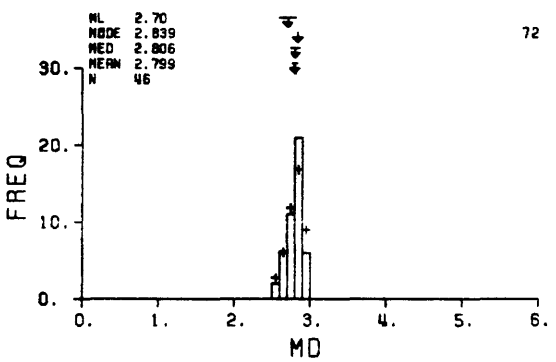
72
ML 2.70
MODE 2.839
MED 2.806
MEAN 2.799
N 46
FREQ
30.
20.
10.
0.
0. 1. 2. 3. 4. 5. 6.
MD

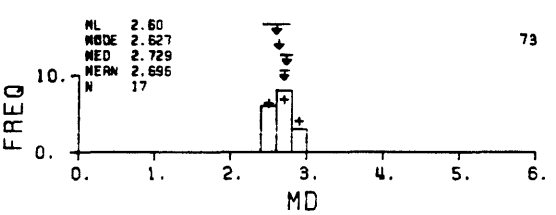
73
ML 2.60
MODE 2.627
MED 2.729
MEAN 2.696
N 17
FREQ
10.
0.
0. 1. 2. 3. 4. 5. 6.
MD

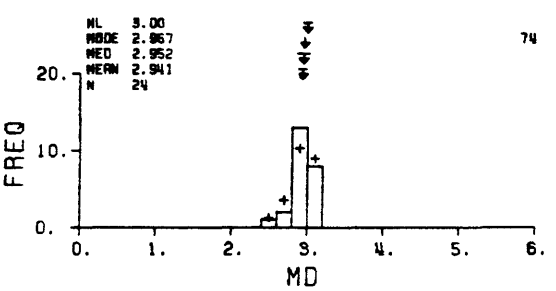
74
ML 3.00
MODE 2.867
MED 2.952
MEAN 2.941
N 24
FREQ
20.
10.
0.
0. 1. 2. 3. 4. 5. 6.
MD

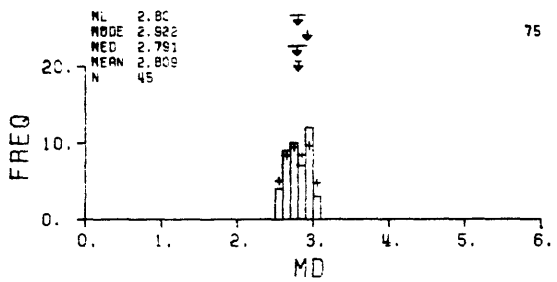
ML 2.80
MODE 2.922
MED 2.791
MEAN 2.809
N 45
75
FREQ
MD

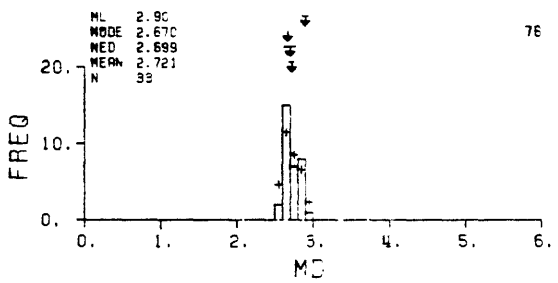
ML 2.90
MODE 2.670
MED 2.699
MEAN 2.721
N 38
76
FREQ
MD

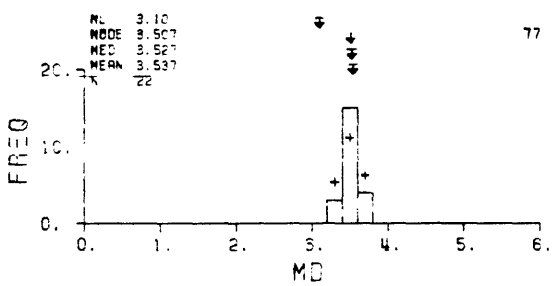
ML 3.10
MODE 3.507
MED 3.527
MEAN 3.537
N 22
77
FREQ
MD

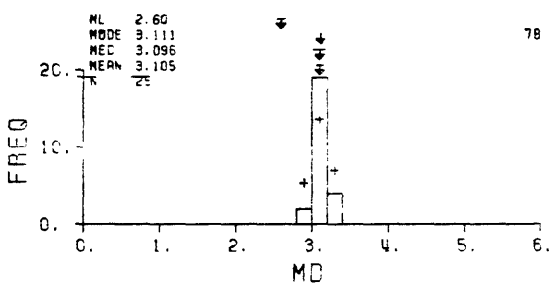
ML 2.60
MODE 3.111
MED 3.096
MEAN 3.105
N 25
78
FREQ
MD

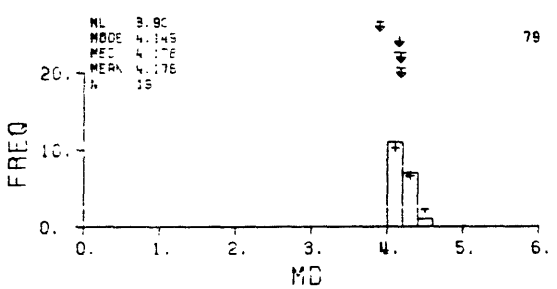
ML 3.90
MODE 4.145
MED 4.178
MEAN 4.178
N 19
79
FREQ
MD

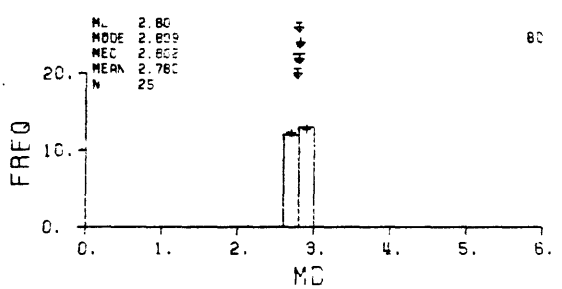
ML 2.80
MODE 2.809
MED 2.802
MEAN 2.780
N 25
80
FREQ
MD

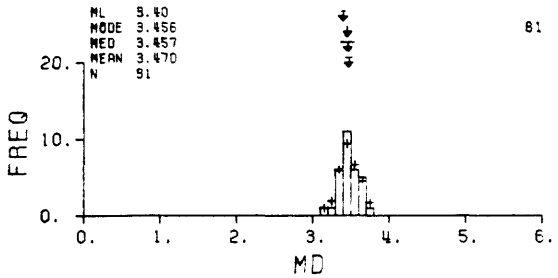
ML 3.40
MODE 3.456
MED 3.457
MEAN 3.470
N 91
B1
FREQ
MD

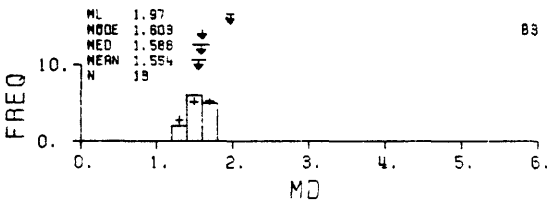
ML 1.97
MODE 1.603
MED 1.588
MEAN 1.554
N 19
B3
FREQ
MD

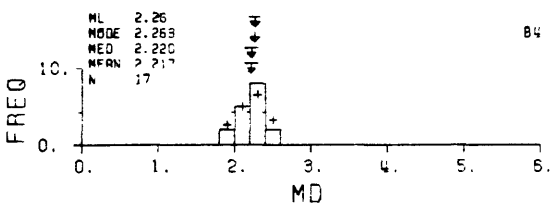
ML 2.26
MODE 2.263
MED 2.220
N 17
B4
FREQ
MD

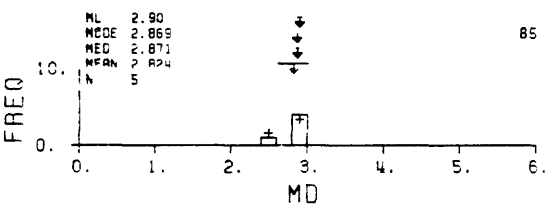
ML 2.90
MODE 2.869
MED 2.871
N 5
B5
FREQ
MD

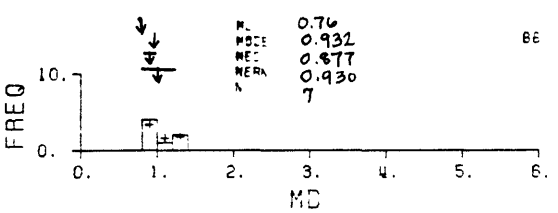
0.76
0.932
0.877
0.930
7
B6
FREQ
MD

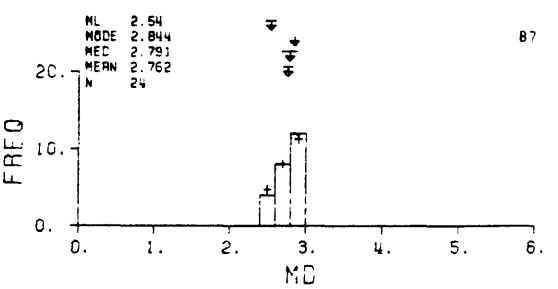
ML 2.54
MODE 2.844
MED 2.791
MEAN 2.762
N 24
B7
FREQ
MD

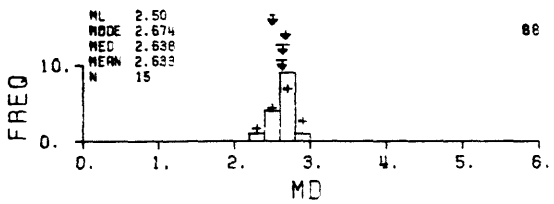
ML 2.50
MODE 2.674
MED 2.638
MEAN 2.683
N 15
88
FREQ
10.
0.
0. 1. 2. 3. 4. 5. 6.
MD

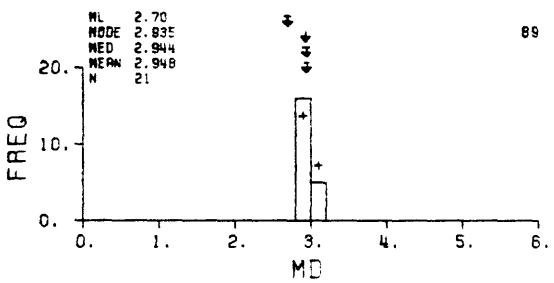
ML 2.70
MODE 2.835
MED 2.944
MEAN 2.948
N 21
89
FREQ
20.
10.
0.
0. 1. 2. 3. 4. 5. 6.
MD

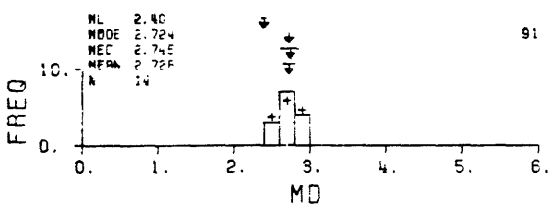
ML 2.40
MODE 2.724
MED 2.745
MEAN 2.728
N 14
91
FREQ
10.
0.
0. 1. 2. 3. 4. 5. 6.
MD

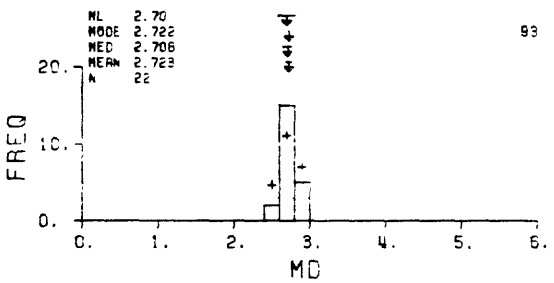
ML 2.70
MODE 2.722
MED 2.706
MEAN 2.723
N 22
93
FREQ
20.
10.
0.
0. 1. 2. 3. 4. 5. 6.
MD

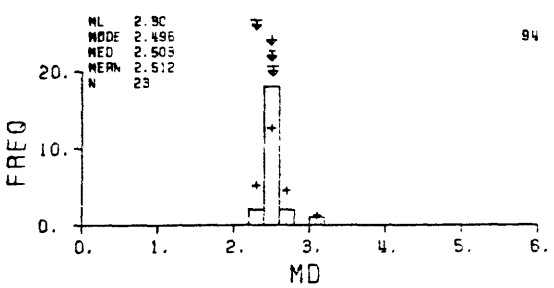
ML 2.90
MODE 2.496
MED 2.503
MEAN 2.512
N 23
94
FREQ
20.
10.
0.
0. 1. 2. 3. 4. 5. 6.
MD

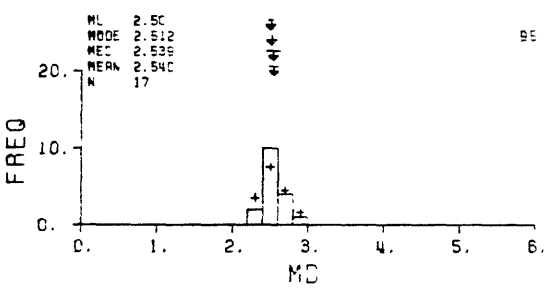
ML 2.50
MODE 2.512
MED 2.539
MEAN 2.540
N 17
95
FREQ
20.
10.
0.
0. 1. 2. 3. 4. 5. 6.
MD

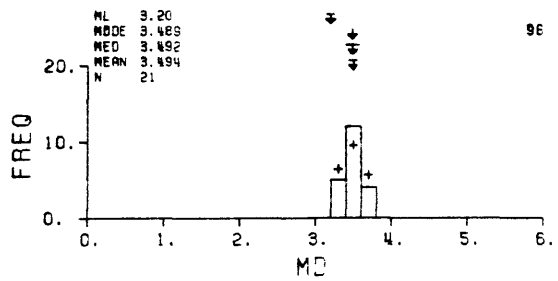
ML 3.20
MODE 3.48S
MED 3.492
MEAN 3.494
N 21
98
FREQ
MD

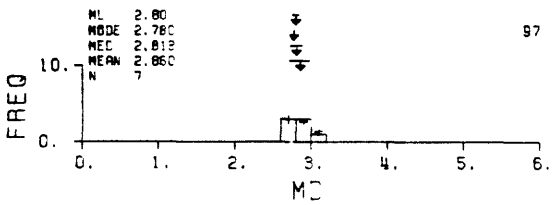
ML 2.80
MODE 2.78C
MED 2.819
MEAN 2.86C
N 7
97
FREQ
MD

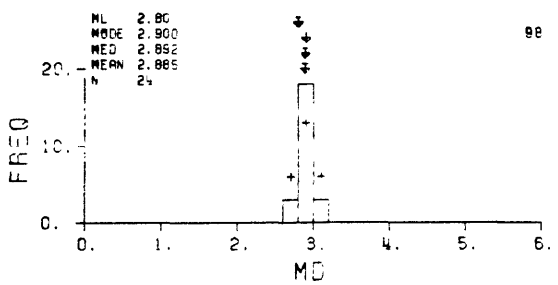
ML 2.80
MODE 2.900
MED 2.892
MEAN 2.885
N 24
98
FREQ
MD

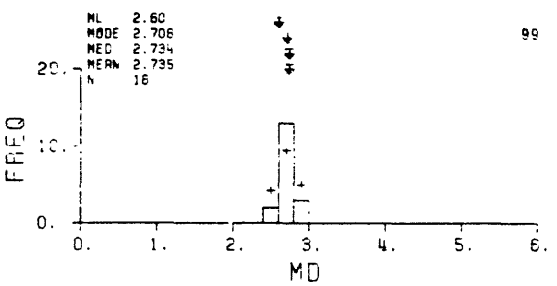
ML 2.60
MODE 2.706
MED 2.734
MEAN 2.735
N 16
99
FREQ
MD

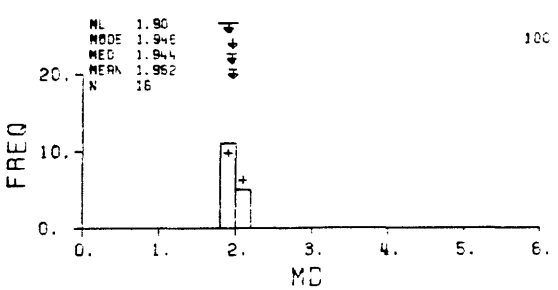
ML 1.90
MODE 1.94E
MED 1.944
MEAN 1.952
N 16
100
FREQ
MD

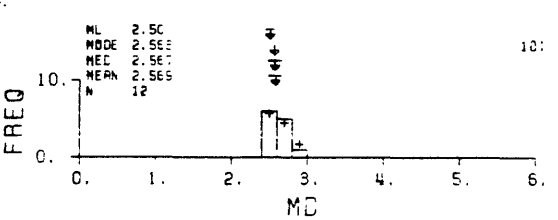
ML 2.5C
MODE 2.56E
MED 2.56[illegible]
MEAN 2.565
N 12
10[illegible]
FREQ
MD

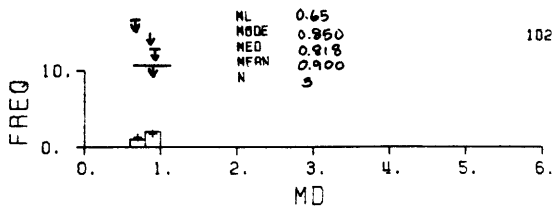
ML 0.65
MODE 0.950
MED 0.918
MEAN 0.900
N 3
102
FREQ
10.
0.
0. 1. 2. 3. 4. 5. 6.
MD

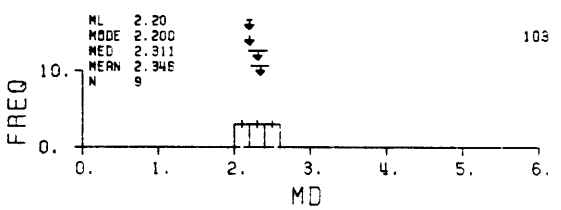
ML 2.20
MODE 2.200
MED 2.311
MEAN 2.348
N 9
103
FREQ
10.
0.
0. 1. 2. 3. 4. 5. 6.
MD

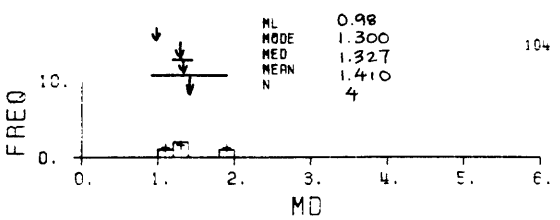
ML 0.98
MODE 1.300
MED 1.327
MEAN 1.410
N 4
104
FREQ
10.
0.
0. 1. 2. 3. 4. 5. 6.
MD

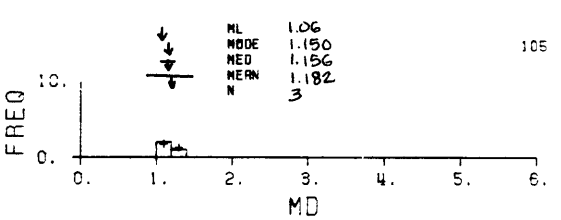
ML 1.06
MODE 1.150
MED 1.156
MEAN 1.182
N 3
105
FREQ
10.
0.
0. 1. 2. 3. 4. 5. 6.
MD

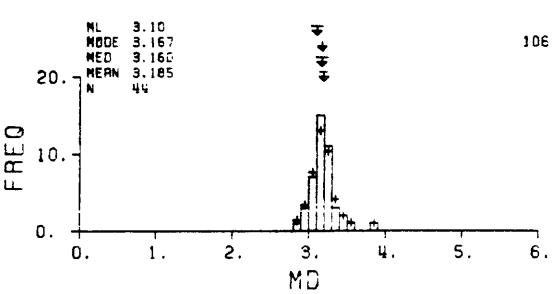
ML 3.10
MODE 3.167
MED 3.160
MEAN 3.185
N 44
106
FREQ
20.
10.
0.
0. 1. 2. 3. 4. 5. 6.
MD

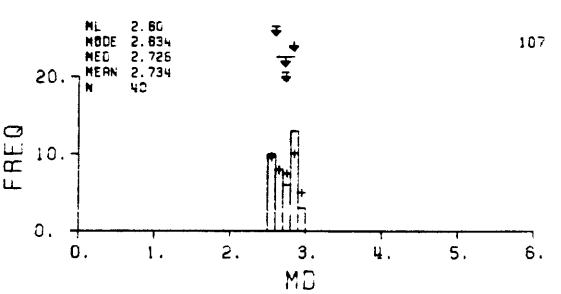
ML 2.80
MODE 2.834
MED 2.726
MEAN 2.734
N 40
107
FREQ
20.
10.
0.
0. 1. 2. 3. 4. 5. 6.
MD

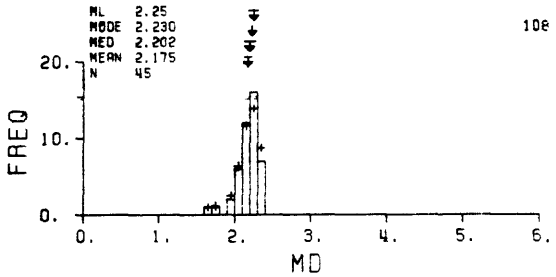
ML 2.25
MODE 2.230
MED 2.202
MEAN 2.175
N 45
108
FREQ
MD

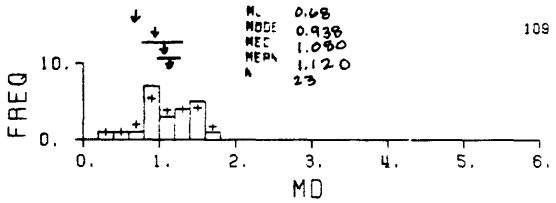
ML 0.68
MODE 0.938
MED 1.080
MEAN 1.120
N 23
109
FREQ
MD

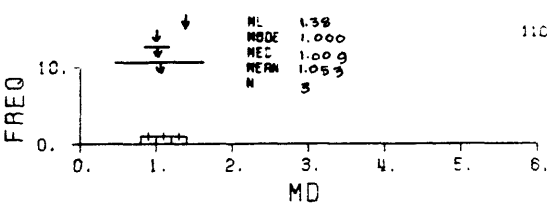
ML 1.38
MODE 1.000
MED 1.009
MEAN 1.053
N 3
110
FREQ
MD

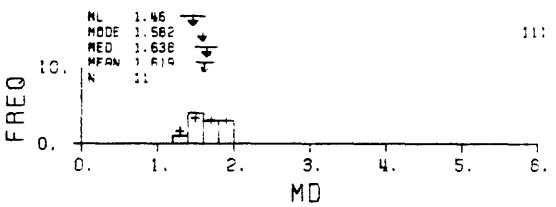
ML 1.46
MODE 1.562
MED 1.638
MEAN 1.619
N 11
111
FREQ
MD

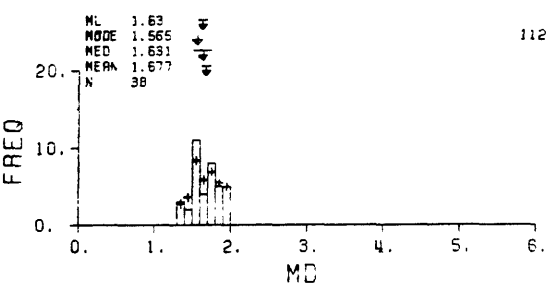
ML 1.63
MODE 1.565
MED 1.631
MEAN 1.677
N 38
112
FREQ
MD

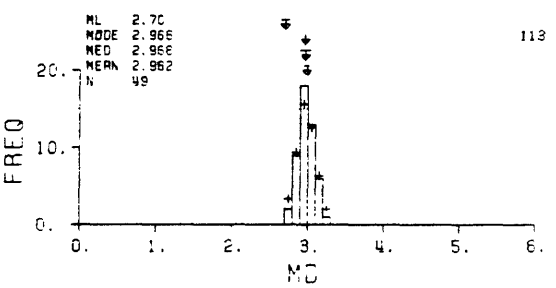
ML 2.70
MODE 2.966
MED 2.966
MEAN 2.962
N 49
113
FREQ
MD

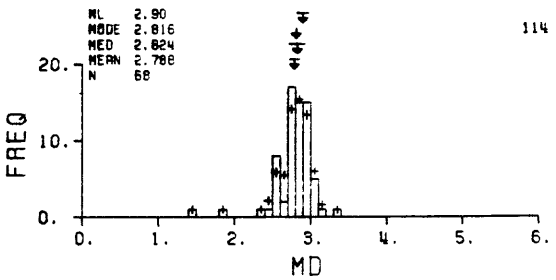
ML 2.90
MODE 2.816
MED 2.824
MEAN 2.788
N 68
114
20.
10.
0.
FREQ
0.
1.
2.
3.
4.
5.
6.
MD

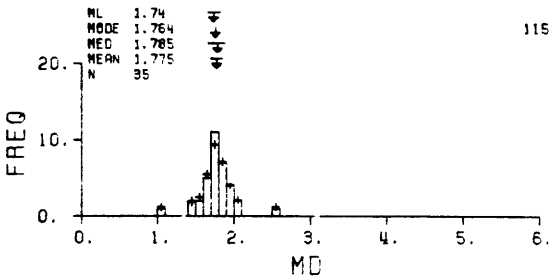
ML 1.74
MODE 1.764
MED 1.785
MEAN 1.775
N 95
115
20.
10.
0.
FREQ
0.
1.
2.
3.
4.
5.
6.
MD